Phase coexistence in the mixed crystal Rb1-x(NH4)xH2AsO4
by Nicholas Joaquim Pinto

A thesis submitted in partial fulfillment of the requirements for the degree of Doctor of Philosophy in Physics
Montana State University

Abstract:
A study of the coexistence phenomenon in mixed crystals of rubidium ammonium dihydrogen arsenate has been done. Coexistence in this study refers to the simultaneous presence of ferroelectric and proton glass phases as temperature is lowered below the ferroelectric phase transition temperature Tc. Such coexistence is found to exist in these mixed crystals only for small ammonium concentrations. Our results show that coexistence exists for lower ammonium concentration than previously suggested. A study was also done on crystals with larger ammonium concentrations that show pure proton glass behavior and the results compared with the coexistence phenomenon.

Dielectric, spontaneous polarization and nuclear magnetic resonance experiments on mixed crystals with small ammonium concentrations show that at low temperatures there exists intimate coexistence of ferroelectric clusters with proton glass clusters below the glass transition temperature Tg. In the proton glass phase, we observe a spread of relaxation times due to the creation and annihilation of HAsO4 and H3AsO4 pairs as they diffuse through the crystal. Spin lattice relaxation times for the acid deuterons in a 10% ammoniated sample show a broad T1 minimum near the glass transition temperature which is characteristic of proton glasses. Field-cooling experiments were also done on the pure proton glass. The results are consistent with dielectric measurements, but the remanent polarization was found to be extremely small. This polarization was found to depend on the rate of heating and cooling the sample while performing the experiment.

PHASE COEXISTENCE in the MIXED CRYSTAL $Rb_{1-x}(NH_4)_xH_2AsO_4$

by

Nicholas Joaquim Pinto

A thesis submitted in partial fulfillment
of the requirements for the degree

of

Doctor of Philosophy

in

Physics

MONTANA STATE UNIVERSITY
Bozeman, Montana

November 1992

APPROVAL

of a thesis submitted by

Nicholas Joaquim Pinto

This thesis has been read by each member of the thesis committee and has been found to be satisfactory regarding content, English usage, format, citations, bibliographic style, and consistency, and is ready for submission to the College of Graduate Studies.

Nov. 4, 1992
Date

V. Hugo Schmidt
Chairperson, Graduate Committee

Approved for the Major Department

Nov 4, 1992
Date

Head, Major Department

Approved for the College of Graduate Studies

11/17/92
Date

Graduate Dean

STATEMENT OF PERMISSION TO USE

In presenting this thesis in partial fulfillment of the requirements for a doctoral degree at Montana State University, I agree that the Library shall make it available to borrowers under rules of the Library. I further agree that copying of this thesis is allowable only for scholarly purposes, consistent with "fair use" as prescribed in the U.S. Copyright Law. Requests for extensive copying or reproduction of this thesis should be referred to University Microfilms International, 300 North Zeeb Road, Ann Arbor, Michigan 48106, to whom I have granted "the exclusive right to reproduce and distribute copies of the dissertation in and from microfilm and the right to reproduce by abstract in any format."

Signature Nicholas Lints

Date 11-4-92

ACKNOWLEDGEMENTS

I am very thankful to all the people in the physics department for their kindness and help during my stay as a graduate student at Montana State University. I sincerely thank my advisor Hugo Schmidt for his support and discussions that have given me a deeper understanding of hydrogen bonded ferroelectrics. To Toby Howell, thanks a million for teaching me the "nuts and bolts" of nuclear magnetic resonance, your assistance in helping me become an experimental physicist is greatly appreciated. I am also grateful to all the people who visited our lab, for their support and encouragement. Of special mention is George Tuthill, Jack Drumheller, Stuart Hutton (Stu) and Stefan Waplak.

Finally, I would like to thank Erik Andersen, Norm Williams and Mark Baldwin for their assistance and friendship.

TABLE OF CONTENTS

TABLE OF CONTENTS - Continued

LIST OF TABLES

LIST OF FIGURES

LIST OF FIGURES - Continued

LIST OF FIGURES - Continued

LIST OF FIGURES - Continued

LIST OF FIGURES - Continued

ABSTRACT

A study of the coexistence phenomenon in mixed crystals of rubidium ammonium dihydrogen arsenate has been done. Coexistence in this study refers to the simultaneous presence of ferroelectric and proton glass phases as temperature is lowered below the ferroelectric phase transition temperature T_c. Such coexistence is found to exist in these mixed crystals only for small ammonium concentrations. Our results show that coexistence exists for lower ammonium concentration than previously suggested. A study was also done on crystals with larger ammonium concentrations that show pure proton glass behavior and the results compared with the coexistence phenomenon.

Dielectric, spontaneous polarization and nuclear magnetic resonance experiments on mixed crystals with small ammonium concentrations show that at low temperatures there exists intimate coexistence of ferroelectric clusters with proton glass clusters below the glass transition temperature T_g. In the proton glass phase, we observe a spread of relaxation times due to the creation and annihilation of $HAsO_4$ and H_3AsO_4 pairs as they diffuse through the crystal. Spin lattice relaxation times for the acid deuterons in a 10% ammoniated sample show a broad T_1 minimum near the glass transition temperature which is characteristic of proton glasses. Field-cooling experiments were also done on the pure proton glass. The results are consistent with dielectric measurements, but the remanent polarization was found to be extremely small. This polarization was found to depend on the rate of heating and cooling the sample while performing the experiment.

CHAPTER 1

INTRODUCTION

Investigation of the proton glass rubidium ammonium dihydrogen arsenate ($Rb_{1-x}(NH_4)_xH_2AsO_4$-RADA) and its deuterated counterpart ($Rb_{1-x}(ND_4)_xD_2AsO_4$-DRADA) has been carried out to understand the coexistence of ferroelectric and proton glass phases as temperature is lowered below the ferroelectric transition temperature T_c. Above this temperature the system is in the paraelectric phase. Below the transition temperature, for x=0 the system is ferroelectric below T_c and for x=1 the system is antiferroelectric below the Néel temperature T_N. For a range of intermediate x-values shown in the phase diagram in Fig. 1, the system makes a smooth transition to the "proton glass" phase. This "transition" to the glassy phase is <u>not</u> a thermodynamic phase transition. Rather, it is an effect seen due to competing ferroelectric and antiferroelectric interactions as a frequency dependent freezing of protons in their bond sites as temperature is lowered. The region on the phase diagram where one observes a dispersion in the

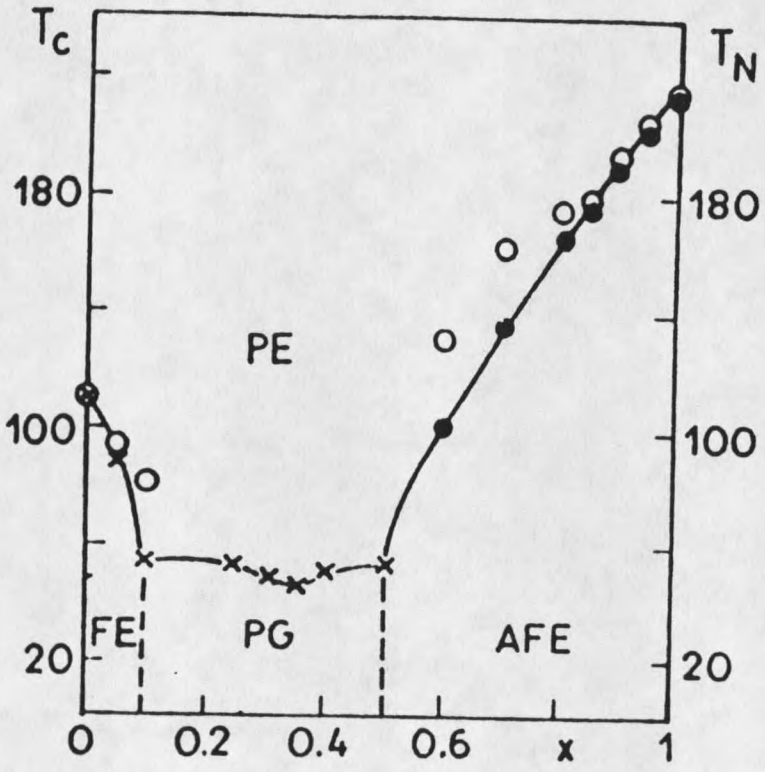

Figure 1. Phase diagram of RADA mixed crystals as a function of ammonium concentrations (x) and temperature. PE, FE, PG and AFE denote paraelectric, ferroelectric, proton glass and antiferroelectric phases respectively.[1]

dielectric response is called the "proton glass" phase. Such a phase diagram shows the boundaries between the paraelectric (PE) and ferroelectric (FE) phase for small ammonium (x) concentrations and the boundary between the PE and antiferroelectric (AFE) phase for large x values. Our experiments concentrate on crystals having ammonium concentrations (x) close to the ferroelectric side of the phase diagram.

Proton glass was first discovered by E. Courtens[2] in 1982 in the mixed crystal rubidium ammonium dihydrogen phosphate (RADP) with x=0.34. In this system, the frustration that leads to glassy behavior results from the random placement of the NH_4^+ cation. To understand the role of the NH_4^+ cation, it is important to understand the origin of ferroelectricity and antiferroelectricity in the pure crystals. The most widely studied ferroelectric crystal in this family of crystals is KH_2PO_4 (KDP). In the case of the antiferroelectric crystals it is $(NH_4)H_2PO_4$ (ADP). In the crystals studied here the following substitution must be made, Rb for K and As for P. The procedure used to grow these crystals is given in Chapter 2. These crystals are tetragonal in their structure with the ferroelectric or antiferroelectric axis along the c direction of the crystal.

Fig. 2 shows the crystal structure of KDP[3] at room

temperature and Fig. 3 is its c-axis projection in the ferroelectric ordered phase.[4] The structure consists of two interpenetrating sublattices. One is a body-centered sublattice of PO_4 tetrahedra and the other a body-centered sublattice of K^+ ions. The K^+ and P^{5+} ions are alternately arranged in chains running along the c axis and are spaced from each other by a distance c/4. Each phosphorus ion is surrounded by four oxygen ions at the corners of a tetrahedron and each PO_4 group is hydrogen bonded to four other PO_4 groups via 'acid' hydrogen bonds. Because these PO_4 neighbors in adjacent chains are c/4 higher or lower than the PO_4 in question, the linkage is such that there is an O...H-O 'acid' hydrogen bond between the one 'upper oxygen' of one PO_4 group and one 'lower oxygen' of a PO_4 group spaced c/4 above the previous one. These hydrogen bonds are nearly perpendicular to the c axis. Neutron diffraction studies show that only two hydrogen atoms are located near a PO_4 group making it as a whole an $(H_2PO_4)^-$ ion. Neutron diffraction studies also show that the hydrogen atoms are statistically distributed at the center of the O-H...O bonds in the paraelectric phase while in the ferroelectric phase the protons are statistically off center in the hydrogen bond. In this phase, the protons are ordered in such a way that in a single domain the protons are either close to the 'upper oxygen' or 'lower oxygen'

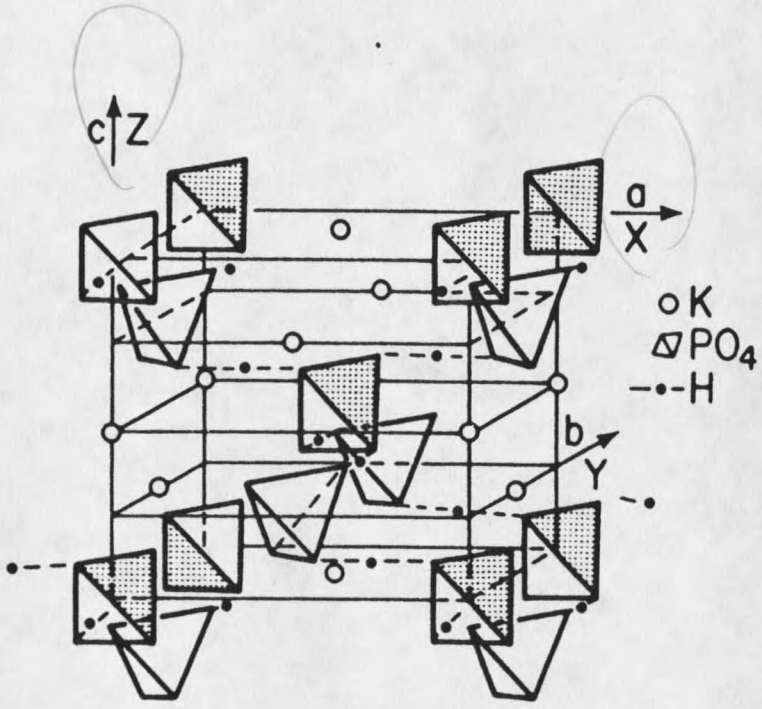

Figure 2. The crystal structure of KDP at room temperature.[3]

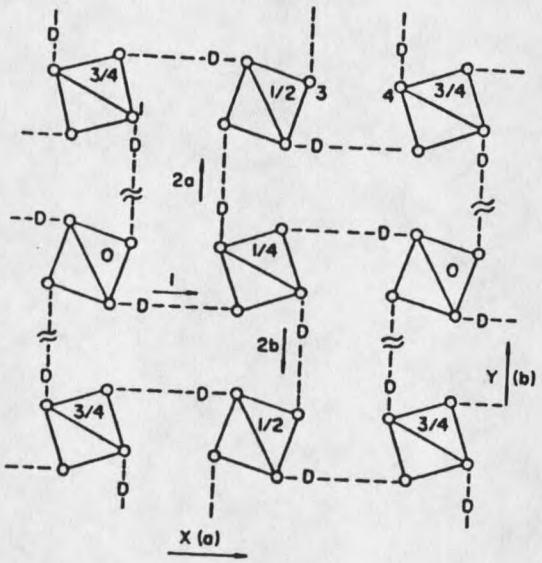

Figure 3. c-axis projection of KDP in the ferroelectric phase.[4]

depending on the polarity. This ordering effect of the protons around the PO_4 tetrahedron is the key factor responsible for ferroelectricity in these crystals. In this ordered state the polarization arises from the displacements of K^+ and P^{5+} ions in the direction of the c axis as shown in Fig.4. The direction of the spontaneous polarization is along the P^{5+} displacement. Thus, when the polarization is 'up', these protons are nearest to the 'lower oxygen' ions of each PO_4 group and vice versa.

The antiferroelectric counterpart has NH_4^+ substituted for K^+ and as a result the 'ammonium' protons are hydrogen bonded to the oxygens in addition to the 'acid' protons. Two of the 'ammonium' protons form 'short' bonds with the surrounding PO_4 tetrahedra and two 'long' as seen in Fig. 5. This has an influence on the position of the 'acid' proton in its O-H...O bond. In the antiferroelectric phase the arrangement of the 'acid' protons is such that each PO_4 tetrahedron has a proton at the upper and at the lower end unlike in KDP where in the ferroelectric phase all the 'acid' protons were attached either to the top or bottom of the PO_4 tetrahedron. Such an arrangement of the protons results in the polarization alternately pointing in the 'up' and 'down' directions as seen in Fig. 6 yielding a net polarization of zero. The arrows indicate the direction of polarization in a unit cell.

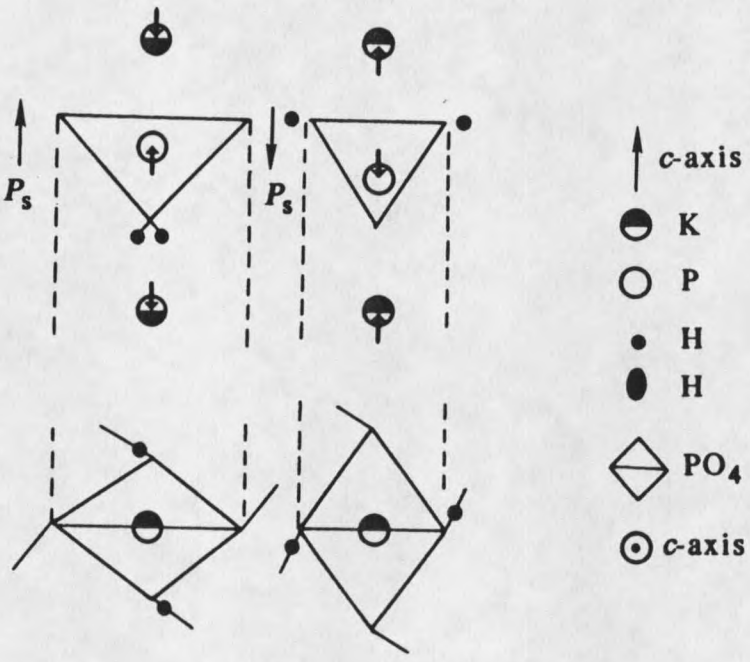

Figure 4. Schematic representation of the dipole moment in KDP. Polarization along the c axis.[5]

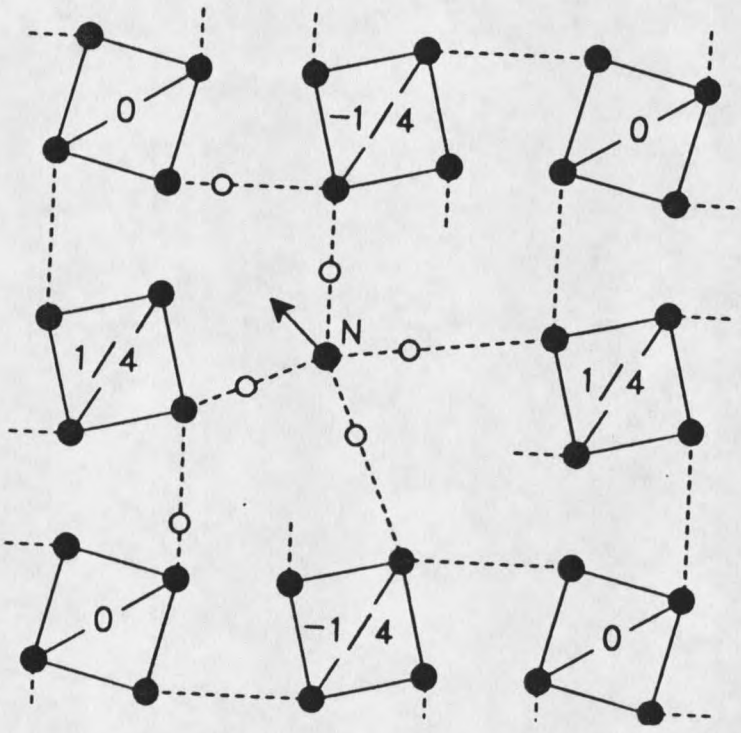

Figure 5. Structure of a mixed crystal of RADA showing a NH_4^+ ion that replaced a Rb atom along the c axis. A NH_4^+ at height 0 is shown attached to nearby oxygens of a AsO_4 tetrahedra. The heights in units of c of the arsenate centers of the AsO_4 tetrahedra are indicated. The offcenter motion of the ammonium ion is indicated by the arrow. this results in the formation of two long and two short bonds with the surrounding AsO_4 tetrahedra.[6]

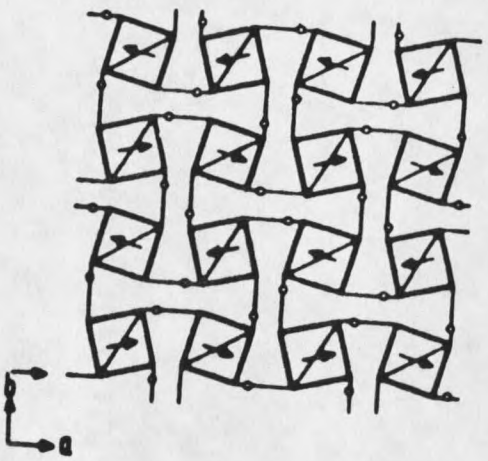

Figure 6. Schematic representation of the antiferroelectric phase of ADP.[7]

In the mixed RADA system the ammonium cation substitutes at random into the Rb sites. There are thus regions within the crystal that have rich ammonium concentrations and hence a greater tendency to order antiferroelectrically while in the rubidium-rich regions the ordering tendency would be more ferroelectric. Analogous to spin-glass and pseudo-spin glass where glassy behavior is generally considered to require randomness and frustration, in proton glass the randomness lies in the Rb^+ and NH_4^+ cation placement. The frustration lies in two inconsistent tendencies for ordering of the O-H...O proton "pseudospins". Analogous to KDP mentioned above, in ferroelectric RbH_2AsO_4 (RDA) if one looks down along c, the protons in O-H...O bonds lying along a(b) are near the tops(bottoms) of AsO_4 groups, or vice versa for reversed domains. Similarly, in antiferroelectric $NH_4H_2AsO_4$ (ADA) two adjacent N-H...O bonds (viewed along c) of a given NH_4^+ ion are short and the other two adjacent N-H...O bonds are long. A given O-H...O bond shares oxygens with one short and one long N-H...O bond, with the O-H near the long bond and the H...O near the short bond. This arrangement puts one proton near the top, and one near the bottom, of each AsO_4 group, analogous to ADP, which is inconsistent with ferroelectric ordering. In a mixed crystal, these inconsistent ordering schemes favored by the arsenate and

ammonium ions cause frustration and inhibit or prevent either ferroelectric or antiferroelectric ordering and lead to glassy behavior. The ammonium cation thus plays an important role in the occurrence of glassy behavior in these samples.

The nature of the coexistence regions is still not clear. In this work we undertake to explain this question by performing three different experiments on crystals with ammonium concentrations close to the ferroelectric/proton glass phase boundary and a fourth experiment on a crystal which exhibits only glassy behavior. We believe that in the coexistence region there are interpenetrating regions of ferroelectric and paraelectric/proton glass clusters that are intimately interlocked with short correlation lengths. These correspond to regions that have excess rubidium or ammonium density.

First evidence of coexistence in proton glasses was seen in the phosphates by Takashige et al.[8] for x=0.75. They labelled this behavior as re-entrant, indicating the presence of a new phase that the system "enters" after entering into the antiferroelectric phase as temperature is lowered below T_N. In the arsenates, coexistence was first observed by Trybula et al.[9] Proton glass behavior is present for ammonium concentrations in the range $0.04<x<0.50$ while coexistence of ferroelectric and proton

glass phases is seen in the range $0.04<x<0.15$. This work extends the results of Trybula et al.[9] to lower ammonium concentrations and to other experiments besides measurements of the complex dielectric constant.

The first three experiments (dielectric, spontaneous polarization and field cooled) investigate bulk response of the sample to applied electric fields along different crystallographic axes. The last experiment is nuclear magnetic resonance (NMR) on a single crystal of DRADA. Both deuterated and undeuterated samples were used in the study of dielectric properties and spontaneous polarization, while only deuterated samples were used in the field cooled and nuclear magnetic resonance experiments. The dielectric measurements were carried out at low applied electric fields (typically 5 V/cm) and a range of frequencies. These results clearly show the presence of the proton glass phase coexisting with the ferroelectric phase for certain ammonium concentrations. A phase diagram is presented for ammonium concentrations close to the ferroelectric/proton glass boundary. Coexistence could not be detected for ammonium concentration less than 1% via dielectric measurements. It is suggested that a more sensitive technique like NMR be performed. Spontaneous polarization measurements indicate that the ferroelectric transition in the pure sample is first order while for the mixed sample

the spontaneous polarization rises gradually below T_c in agreement with the results from dielectric measurements. NMR studies give more information about the dynamics involved during phase transitions. These effects are seen in the spin lattice relaxation rates and in the NMR spectrum.

Finally, it must be pointed out that these glasses are worth studying as they fall in a category between that of spin glasses that have well developed theories and window glasses that are less understood. It is hoped that spin glass theory can be extended to explain more rigorously proton glass behavior and eventually explain the dynamics governing window glass.

CHAPTER 2

CRYSTAL GROWTH

Crystals are ordered arrays of atoms. In perfect crystals, these arrays repeat themselves in a periodic manner on a regular lattice. A unit cell is the fundamental building block of the crystal. It retains all the properties of the bulk crystal that one usually measures in an experiment. In practice it very difficult to grow a single crystal that is perfect. Most crystals will grow with some form of imperfection in their crystal structure. Essentially there are three classes of defects,[10] point defects, line defects and sheet defects. One can only minimize these defects by exercising proper care during the growth process.

All of the crystals grown for the purpose of this thesis were obtained by controlled evaporation of the proper solution. The solvent used for the undeuterated crystals was plain water while for the deuterated crystals the solvent was heavy water. Such a "solution growth" system is binary or a two component system (solute +

solvent) and so requires simultaneous control of two parameters, temperature and concentration during the crystallization process. Frequent checks on the acidity of the solution were made using color coordinated Ph testers. A solution that was acidic resulted in the growth of crystals that were long and needle-like. Best results occurred from solutions that were neutral. Adding a base to an acidic solution shifts the acidity towards the neutral state and vice versa. Caution must be taken while adding the neutralizing agent to avoid the possibility of making a new solution that differs from the original solution. For eg. in the growing of KADA, if the solution is too acidic then the bases KOH and $(NH_4)OH$ must be added in the right amounts to maintain the concentrations of K^+ and NH_4^+ ions the same as in the original solution. Evaporation is best achieved by pouring the solution into special evaporating dishes where there is a better balance in the volume of liquid and the evaporation rate as compared to say a beaker that has more depth than width in its construction.

Mixed crystals of RADA for all the ammonium concentrations reported here were obtained by slow evaporation of aqueous solution of RbH_2AsO_4 (RDA) and $(NH_4)H_2AsO_4$ (ADA) mixed in the proper molar ratios. The generic notation for these mixed crystals for an x concentration of ammonium is $Rb_{1-x}(NH_4)_xH_2AsO_4$. The deuterated

crystals were grown under an atmosphere of argon to maintain a high percentage of deuteration since the ferroelectric transition temperature is sensitive to the degree of deuteration of the crystal. The following steps were taken in the growth of RADA with x=0.1. RADA with x=0.1 is prepared by mixing 90% of RDA with 10% of ADA in water and letting the solution evaporate slowly.

(1) Growth of RDA:

Chemical Reaction: $Rb_2CO_3 + As_2O_5 + 2H_2O \rightarrow 2RbH_2AsO_4 + CO_2$

In order to follow this reaction, proper care must be taken to add the chemicals in the right amount. Rubidium carbonate has a molecular weight of 230.950 gm and arsenic pentoxide has a molecular weight of 229.840 gm. In a 1:1 molar ratio one needs to add the above amounts in a beaker and dissolve it in water (for deuterated RDA heavy water is added instead). Smaller amounts, say $1/10^{th}$ mole, would require 23.095 gm of rubidium carbonate and 22.984 gm of arsenic pentoxide. The reaction evolves heat and so water should be added slowly. It is preferable to conduct this experiment under the hood with the beaker partially sitting in a water bath. The residue on complete evaporation is RDA. The molecular weight of RDA is 226.38 gm and must be noted in order to grow mixed crystals involving RDA.

(2) Growth of ADA:

Chemical Reaction: $(NH_4)_2CO_3 + As_2O_5 + 2H_2O \rightarrow 2(NH_4)H_2AsO_4 + CO_2$

In order to follow this reaction, proper care must be taken to add the chemicals in the right amount. Ammonium carbonate has a molecular weight of 96.081 gm and arsenic pentoxide has a molecular weight of 229.840 gm. In a 1:1 molar ratio one needs to add the above amounts in a beaker and dissolve it in water (for deuterated ADA heavy water is added instead to deuterated ammonium carbonate which is commercially available). Smaller amounts, say $1/10^{th}$ mole, would require 9.608 gm of ammonium carbonate and 22.984 gm of arsenic pentoxide. The reaction evolves heat and so water should be added slowly. It is preferable to conduct this experiment under the hood with the beaker partially sitting in a water bath. The residue on complete evaporation is ADA. The molecular weight of ADA is 158.920 gm and must be noted in order to grow mixed crystals involving ADA.

(3) Growth of RADA with x=0.1:

To grow RADA with x=0.1, since the molecular weight of RDA is 226.38 gm and that of ADA is 158.920 gm one needs to add

(0.9x226.38 gm) 203.742 gm of RDA to (0.1x158.920 gm) 15.892 gm of ADA and dissolve the mixture in water (or heavy water for deuterated crystals). Making smaller amounts would involve scaling these values accordingly. Upon controlled evaporation, crystals will grow mainly along the ferroelectric c axis. These crystals have tetragonal structure. In order to grow other mixed crystals of RADA, proper amounts of RDA and ADA must be added and the same procedure followed as above. The crystal surfaces are best polished by gentle rubbing over a wet filter paper. Silver paint can then be painted on as electrodes using a fine piece of wire or by evaporation in a vacuum chamber.

CHAPTER 3

APPARATUS AND EXPERIMENTS

The apparatus used to perform the experiments in this work consists of equipment purchased from manufacturers and some that was home built. While the dielectric measuring apparatus is simple in its construction and easy to operate, the nuclear magnetic resonance (NMR) apparatus consists of various instruments that make up the NMR spectrometer and requires the adjustment of various parameters to optimize signal to noise ratio. A brief description of the apparatus used in the experiments and the experimental procedure is presented together with a block diagram of the experimental setup where necessary.

Dielectric

Measurement of the complex dielectric constant $\varepsilon'-i\varepsilon''$ of the samples was performed in an ac electric field. The capacitance and conductance of the sample were measured as functions of temperature to yield the complex permittivity.

The complex permittivity is frequency dependent and was measured at various frequencies ranging from 10 Hz to 100 kHz along different crystallographic axes. Typical electric fields applied across the crystal range from 1 V/cm to 10 V/cm.

Complex permittivity measurements were made using a Model 6425 Wayne-Kerr component analyzer and a Model 1238 General Radio capacitance bridge. These instruments have an internal oscillator that supply the electric field at various frequencies in addition to measuring the capacitance and conductance. The crystal is first cut along the appropriate axis into a rectangular shape and polished to yield surfaces that are parallel. Typical geometrical capacitances were of the order of 0.1 pF. Silver paint was used as electrodes and was applied to the upper and lower surfaces of the crystal. Simple two-lead measurements were made with the sample connected directly across the instrument. The General Radio capacitance bridge had to be balanced manually by changing standard capacitances and conductances to obtain a null in the in-phase and out-of-phase components of the applied electric field respectively. The Wayne-Kerr component analyzer on the other hand has direct readout of the sample capacitance and conductance and can be controlled by a computer via the general purpose interface bus.

From the measured value of the sample capacitance and conductance, the real and imaginary part of the dielectric constant as a function of temperature T was computed as follows:

$$\varepsilon'(T)=C(T)/C_o \quad \text{and} \quad \varepsilon''(T)=G(T)/\omega C_o$$

where C_o is the geometrical capacitance of the sample, C and G are the sample capacitance and conductance and ω is the angular frequency of the applied electric field. To avoid moisture on the crystal surfaces, it is recommended that dry nitrogen gas be passed over the sample in the dewar as the temperature is lowered and while the measurements are made. Presence of moisture will give erroneous results for the sample conductance and can damage the crystal.

Spontaneous Polarization

Spontaneous polarization measurements were made using a Sawyer-Tower[11] bridge shown in Figure 7(a). A variable voltage ac source (60 Hz) was connected to a step-up transformer that provided the high voltage needed to observe saturated hysteresis loops. The series capacitor (C) was used to monitor the charge developed across the crystal (C_x). The crystal in this case was cut along the c axis which for the ammonium concentrations used in these experiments corresponds to the ferroelectric axis. For

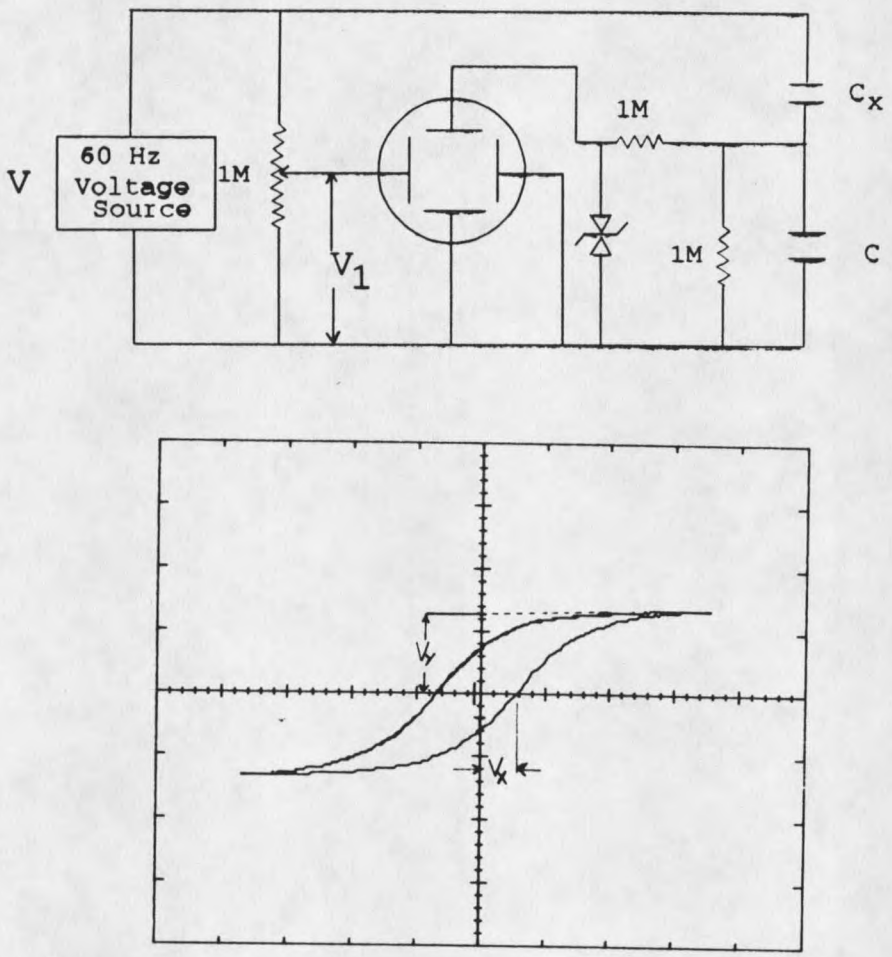

Figure 7. (a) Sawyer-Tower bridge[11] for spontaneous polarization measurements (b) Saturated hysteresis loop showing the voltages used to calculate the spontaneous polarization and coercive field.

these experiments it is *very* important that the electrodes be evaporated on to the surfaces to ensure good electrical contact. If silver paint is used, saturated hysteresis loops cannot be obtained (due to poor electrical contact between the sample and the electrodes) without applying an electric field greater than the dielectric breakdown of the sample. In dielectric measurements the electric field applied was low (~ few V/cm) and applying silver paint worked fine, however in spontaneous polarization measurements, the electric field is substantially higher (~ few kV/cm) and poor contacts would result in arcing and hence poorer electric field homogeneity. The voltage developed across this capacitor (C) is proportional to the charge on the crystal and hence to the spontaneous polarization. It is desirable that the series capacitor have a capacitance of at least a factor of 10 greater than the maximum sample capacitance to ensure that the supply voltage appears directly across the sample with negligible voltage drop across the series capacitor. This capacitor is made variable and must be adjusted to obtain saturated hysteresis loops. A Tektronix oscilloscope with signal averaging capabilities was used to record and plot the saturated hysteresis loops. The series 1 MΩ resistor with the back-to-back zener diode connection is used to prevent high voltages from reaching the y plates of the

oscilloscope in the event that the crystal breaks down electrically and causes a "short" in its path. The parallel 1 MΩ resistor connected across C keeps the RC time constant large so as to avoid any discharge of the capacitor during the experiment but then provides a path for the charge to leak through after the experiment is completed. This way one does not have the capacitor charged to a high potential which could be hazardous. The spontaneous polarization (P_s) and coercive field (E_c) can be obtained from measurements on the hysteresis loops as follows:

$$P_s=CV_y/A \quad \text{and} \quad E_c=V_xV/V_1d$$

where V_x, V_y, V and V_1 are defined in Figs. 7(a) and 7(b) respectively. A is the area of the electrodes and d the thickness of the crystal. It is important also in this experiment that no moisture be allowed to accumulate on the sample.

Field-Cooled and Zero-Field-Cooled

The circuit used in the field-cooling experiment is shown in Fig. 8. The external voltage (V) used in this experiment is a dc source and provides an electric field of 500 V/cm. The electrometer which is connected across the series capacitor (C) has a high input impedance ($> 10^{15}$ Ω) and measures the voltage across C which is proportional to

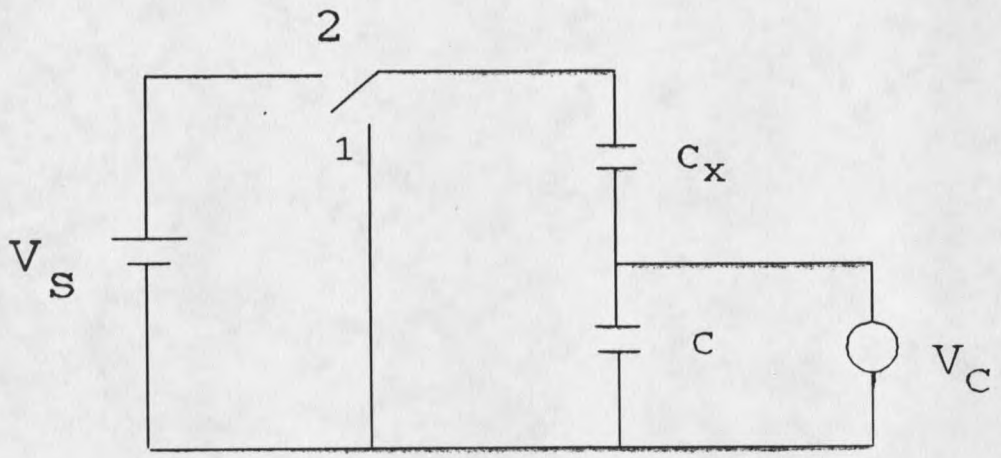

Figure 8. Circuit diagram used for field-cooling experiments.

the charge developed across the crystal (C_x). It is important to use an electrometer with a high input impedance to avoid loading the circuit as the polarization current in these samples is very small. The crystal used in this experiment was a deuterated sample of DRADA with x=0.28. This puts the crystal in the pure proton glass regime of the phase diagram shown in Fig. 1 of Chapter 1. Silver electrodes were evaporated on the surfaces of the crystal that were cut and polished along the tetragonal a axis.

With the switch in position 1 the crystal is cooled below the glass "transition" temperature T_g to about 10 K (i.e. the crystal is zero-field-cooled). The electric field is then applied by throwing the switch to position 2 and the crystal is slowly heated through its glass transition temperature at a constant rate. The sample is heated at the same rate to about 180 K with the electric field still on and then cooled below T_g (i.e. the crystal is field-cooled). At the lowest temperature recorded the switch is once again thrown to position 1 and the crystal heated at the same rate to temperatures above T_g. The voltage recorded by the electrometer is then used to compute the real part of the dielectric constant ε' and remanent polarization P_r as follows:

$$\varepsilon' = CV_c/C_o(V_s - V_c) \quad \text{and} \quad P_r = CV_c/A$$

where V_o and V_s are defined in Fig. 8. C_o is the geometrical capacitance of the sample and A the area of the electrodes. Since the sample used was a pure proton glass the remanent polarization generated by field cooling is much smaller than the spontaneous polarization obtained in the samples used in the previous experiment.

Nuclear Magnetic Resonance

A block diagram of the NMR spectrometer is shown in Fig. 9. It is a pulsed spectrometer using a Kalmus linear pulse amplifier capable of amplifying rf pulses to 150 watts. This amplifier is gated using a pulse programmer. A PTS-300 frequency synthesizer provides the continuous rf and a Model 625 Matec broadband receiver is used to phase detect the NMR signal. A home built phase shifter[12] provides the phase shifted reference signal required for phase sensitive detection. The NMR probe consists of a single coil with a series and parallel capacitor connected close to the coil. The series and parallel capacitor are adjusted to tune the circuit to the Larmor frequency and to have a 50 Ω input impedance. Connecting the capacitors close to the coil was necessary to minimize the effects of stray capacitance of the cables. The capacitors used were high precision tunable capacitors manufactured by Johanson

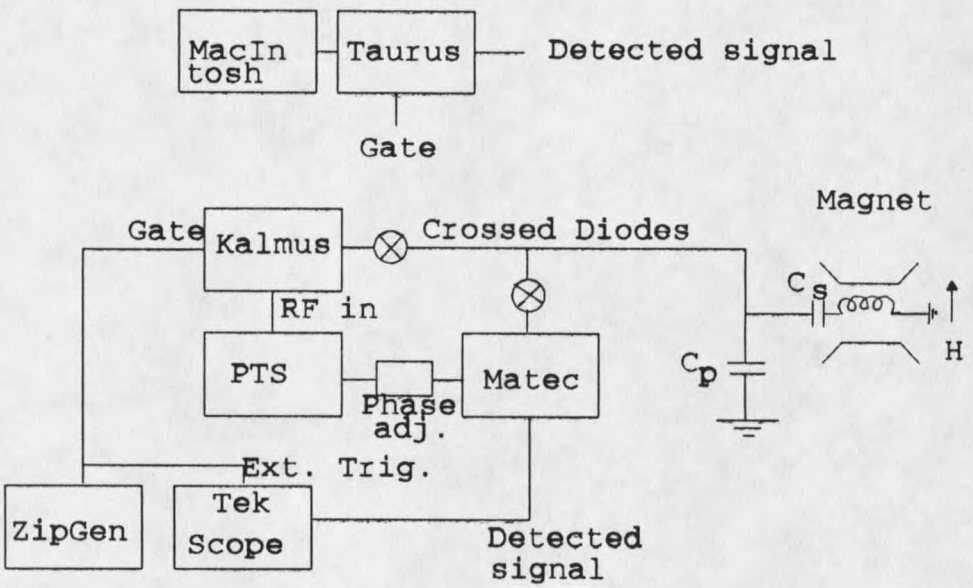

Figure 9. Block diagram of the NMR spectrometer.

Manufacturing[13]. The probe was tuned to 28 MHz for deuterons and matched to 50 Ω to minimize standing waves in the cables. A superconducting magnet was used to provide the magnetic field.

Data acquisition and pulse programming can be achieved in two ways. The Zip-Gen home built pulse programmer is used to gate the amplifier and the detected NMR signal from the Matec receiver is digitized and signal averaged using the Tektronix 2440 oscilloscope. The circuit diagram of this pulse programmer is shown in the Appendix. The NMR spectrometer set up in this way is used to obtain 90° pulses by varying the pulse length to get maximum height of the free induction decay (fid). The spin-lattice relaxation time (T_1) measurements were also made by measuring the height of the fid as a function of pulse separation. Fourier transforms of the fid was obtained by using the Tecmag Taurus instrument with the MacIntosh. This set up replaces the Zip-Gen pulse programmer and oscilloscope. The Tecmag Taurus instrument is run by software from the MacIntosh and provides the gating pulses for the amplifier and signal averages the detected NMR signal from the Matec receiver. The Tecmag Taurus has the option of storing two signals simultaneously thereby making it useful in quadrature detection. This however requires two identical receivers, each set up to detect the in-phase and out-of-

phase components of the fid simultaneously. At the moment we have only one receiver.

In this work we performed deuteron NMR on a single crystal of DRADA with x=0.10. The probe was first tuned using D_2O. This is useful for two reasons, first, it is relatively easy to detect the D_2O nmr signal and second, since there is no quadrupolar splitting the Larmor frequency can be found and then used as the center frequency when studying the DRADA crystal. Since the DRADA sample has both "ammonium" and "acid" deuterons it is important to excite these individually to avoid interference between these two chemically different nuclei. This was accomplished by orienting the crystal in the magnetic field such that the dc magnetic field points along the crystallographic a axis and perpendicular to the ferroelectric c axis. This corresponds to Θ=0° in Fig. 10 where the quadrupolar splitting with the dc magnetic field perpendicular to the ferroelectric c axis in the case of deuterated KDP is shown. In this figure, the "ammonium" deuteron frequency lies along the Θ axis since there is no splitting due to fast reorientations of the ND_4 group. The "acid" deuterons at this orientation are split by 40 kHz and so with a proper choice of the pulse length, it is possible to excite the "ammonium" deuterons only. Likewise the "acid" deuterons can be excited separately by moving

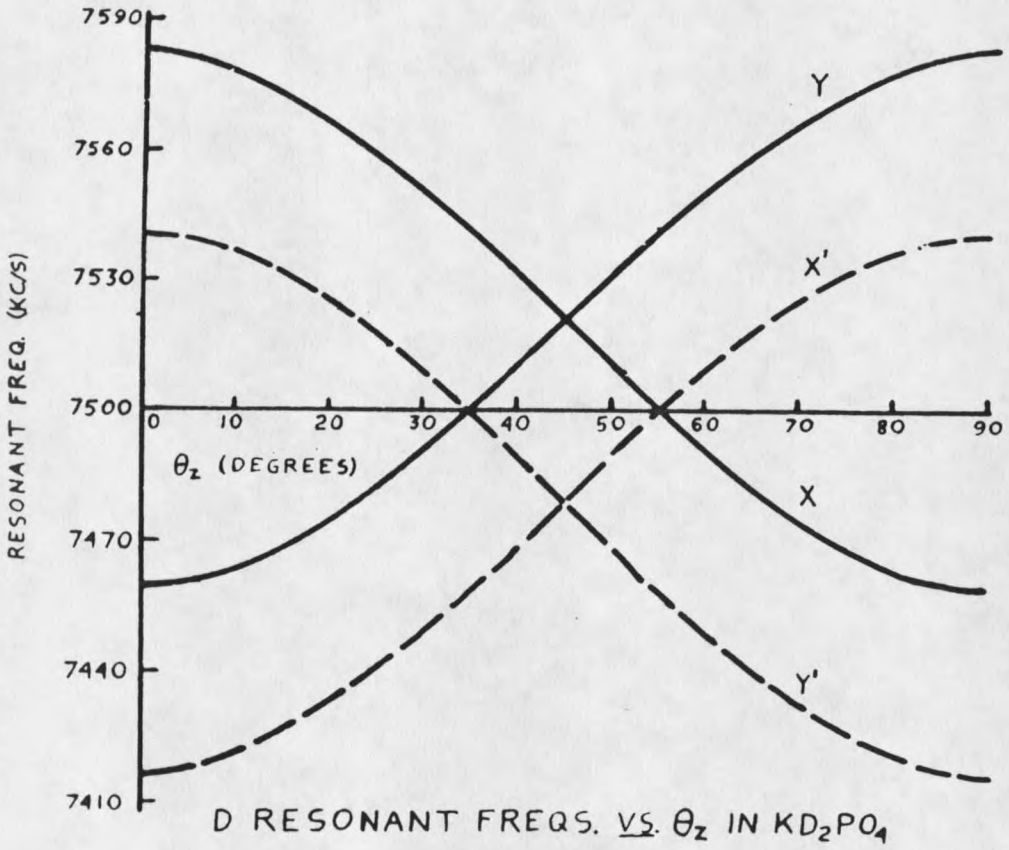

Figure 10. Quadrupolar splitting in deuterated KDP. Deuteron resonant frequencies vs. Θ_z.[14]

40 kHz off resonance and choosing a proper pulse length. The pulse length is chosen so that its power spectrum has negligible contributions beyond 40 kHz. Typical 90° pulse length used in this experiment was 22 μs.

Temperature control was obtained using a continuous flow cryostat with a LakeShore temperature controller model DRC-91C while the sample temperature was measured using a calibrated chromel-alumel type-K thermocouple. Some of the dielectric measurements were carried out in a model RW3 Leybold-Heraeus cold head.

CHAPTER 4

THEORY

Most of the models proposed[15] to explain proton glass behavior are inspired from the spin glass literature. However, unlike spin glasses that do not have random bias fields, in proton glasses the presence of random bias fields is crucial to the occurrence of glassy behavior. The origin of these random fields in proton glasses will be explained together with one of the models proposed that predicts the phase diagram for these glassy systems. Although most models explain the origin of pure proton glass behavior, a model that explains the coexistence of ferroelectric and proton glass phases does not exist as yet.

A proper model for $Rb_{1-x}(NH_4)_xH_2AsO_4$ proton glass must take into account the specific interactions mediated by the NH_4^+ ions since these ions also form hydrogen bonds with the nearby oxygen atoms. As mentioned in chapter 1, two of these bonds are "short" and two are "long" as seen in Fig. 5. Such an interaction has a repulsive effect on the "acid"

protons which bond laterally either to the top or bottom of the AsO_4 tetrahedron. This then competes with ferroelectric ordering in which the "acid" protons are either all attached to the upper corners or all lower corners of the AsO_4 tetrahedron as seen in Fig. 3 of Chapter 1. Such frustrations lead to glassy behavior in these proton glasses. Because the NH_4 groups in these KDP type mixed crystals are positioned nonsymmetrically with respect to the surrounding cations, it tilts the proton double-well potential in a random manner, thus inducing an effective local random field.[16]

It must be mentioned here that the protons in the hydrogen bonds must obey the "ice" rules[17] i.e. i) one and only one proton per hydrogen bond and ii) two protons close to a given arsenate, while the other two bonds linking the arsenate to its neighbors have their protons close to the neighboring arsenates.

The following model[18] for mixed ferro- and antiferroelectric crystals with hydrogen bonds is based on the pseudospin transverse Ising model[15] the Hamiltonian of which is given by:

$$H = -\Omega\sum S_i^x - 1/2\sum J_{ij}S_i^zS_j^z - \sum E_iS_i^z \qquad (4.1)$$

where Ω is the tunneling frequency of the protons between

the two positions in the hydrogen bond (h=1), $E_i/2$ represents the energy splitting of a bond in an applied electric field, S_i^{η} are the pseudospin variables (η=x,y,z) with $S_i^z=\pm 1$ depending whether the proton is at the right or left side of the i^{th} hydrogen bond. These pseudospin operators satisfy the usual commutation relations $[S_i^x, S_j^y]=2iS_i^z\delta_{ij}$ with the normalization $(S_i^{\eta})^2=1$. J_{ij} are random interactions which are assumed[19] to be of infinite range and with a Gaussian probability distribution:

$$P(J_{ij}) = (2\pi J^2)^{-1/2}\exp(-(J_{ij}-J_o)^2/(2J)^2) \qquad (4.2)$$

where $J_o=J_o/N$ is the mean interaction and $J=J/N$ is the distribution width. Here N is the number of pseudospin sites, J_o and J are both concentration dependent, i.e.

$$J_o(x) = -J_o^{AFE}x + J_o^{FE}(1-x) \qquad (4.3)$$

and

$$J(x) = 2[x(1-x)]^{1/2}J_{0.5} \qquad (4.4)$$

where $J_o^{AFE}>0$ and $J_o^{FE}>0$ are parameters appropriate for pure ADA and RDA, whereas $J_{0.5}$ characterizes the 50% RDA-ADA mixture.

The thermal average of S_i^z can be calculated within the mean field approximation (E_i=0) as:

$$\langle S_i^z \rangle = m_i = (H_i^z/2H_i)\tanh(H_i/2kT) \qquad (4.5)$$

where

$$H_i^2 = \Omega^2 + (H_i^z)^2; \quad H_i^z = \sum J_{ij} m_j \qquad (4.6)$$

If the effects of random fluctuations of the tunneling frequency on the proton glass (PG) transition is neglected, then Ω can be considered as a site-independent average value of the transverse field. The fluctuations of Ω would become important however in the case of partially deuterated systems.

At sufficiently low temperature and small tunneling constant Ω, Eq. (4.5) has a solution $m_i=0$ which is in general inhomogeneous owing to J_{ij} being random. The solution depending on couplings J_{ij} is a random field which may be described by its moments $\overline{m}_i$, $\overline{m_i m_j}$, etc., where the bars denote averages with $P(J_{ij})$.

An estimate of the phase-transition temperature can be made by investigating the stability of the paraelectric phase ($m_i=0$) with respect to the spin freezing. First consider the possibility of a phase with $\overline{m}_i \neq 0$ to appear. Note that m_i is in general site-dependent, e.g. in an antiferroelectric phase. Linearizing Eq. (4.5) in m_i we get:

$$m_i = A\sum J_{ij} m_j \quad ; \qquad A = (\Omega/2)\tanh(\Omega/2kT) \qquad (4.7)$$

and averaging over the J_{ij} within the virtual crystal approximation (VCA), i.e. $\overline{J_{ij}m_j}\approx\overline{J}_{ij}\overline{m}_j$, after Fourier transformation (assuming J_{ij} to be translationally invariant), $(1-AJ_q)\overline{m}_q=0$, which yields the transition temperature T_c to a phase, modulated with the wave vector q_o, $\overline{m}_i\sim\cos(q_oR_i)$, we get:

$$kT_c = (\Omega/2)/\operatorname{arctanh}(2\Omega/\overline{J}_{qo}) \quad ; \quad \overline{J}_{qo} = \max \overline{J}_q \tag{4.8}$$

An estimate of the temperature of transition to the structural glass phase with $\overline{m}_i=0$ but $\overline{m_i^2}=0$ can be obtained using an approach commonly used in spin glass theory.[20,21] Squaring Eq.(4.7) and averaging in the VCA with

$$\overline{J_{ik}J_{il}m_km_l}\approx\overline{J_{ik}J_{il}}\,\overline{m_km_l}\approx\overline{J_{ik}J_{il}}\,\overline{m_k^2}\delta_{kl} \tag{4.9}$$

we obtain

$$(1-A^2J_2^2)\overline{m_k^2}=0 \quad ; \quad J_2^2=\sum\overline{J_{ij}^2} \tag{4.10}$$

In Eq.(4.10) we have further supposed that $\overline{m_k^2}$ does not depend on the site. From Eq.(4.10) we note that the paraelectric phase becomes unstable with respect to freezing into the glass phase at the temperature

$$kT=(\Omega/2)/\operatorname{arctanh}(2\Omega/J_2) \tag{4.11}$$

As an example, consider a model in which the sites are randomly occupied by atoms of the kind A or B. For this system we get:

$$\overline{J_{ij}}=X_A^2 J_{ij}^{AA}+2X_AX_BJ_{ij}^{AB}+X_B^2 J_{ij}^{BB} \tag{4.12}$$

where X_A and X_B are the concentrations of the components. For simplicity, choose $J_{ij}^{AA}=-J_{ij}^{BB}>0$, $J_{ij}^{AB}=0$ and suppose a simple cubic lattice with nearest neighbor interactions only. This yields:

$$\overline{J_{qo}}=J_o^{AA}|X_A-X_B|;$$

$$J_o^{AA}=\sum J_{ij}^{AA}; \tag{4.13}$$

$$J_2^2=(J_o^{AA})^2(X_A^2+X_B^2)/6$$

The temperature dependence of the transition to the glass phase depends on the tunnelling constant which is governed by Eq. (4.11) and is shown in Fig. 11.

In the case of RADP mixed systems, supposing we have for RDP $kT_c/\Omega\approx 2$ and $T_c=146$ K, hence $\Omega/k=73$ K and $J_o^{RDP}/k=596$ K. For ADP ($T_c=148$ K) we assume the same tunnelling constant

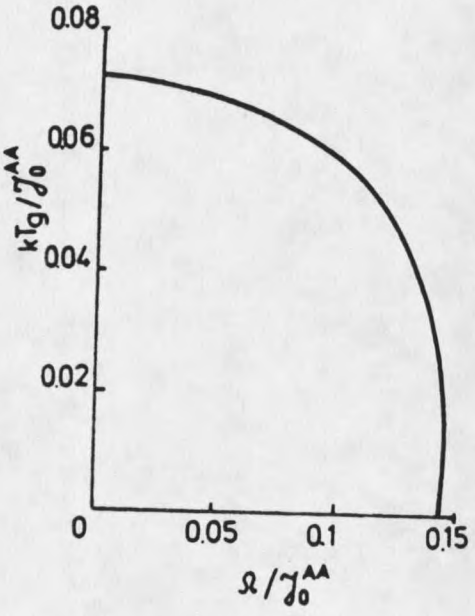

Figure 11. Transition temperature T_g versus the ratio Ω/J_o^{AA} for $x_A=x_B=0.5$.

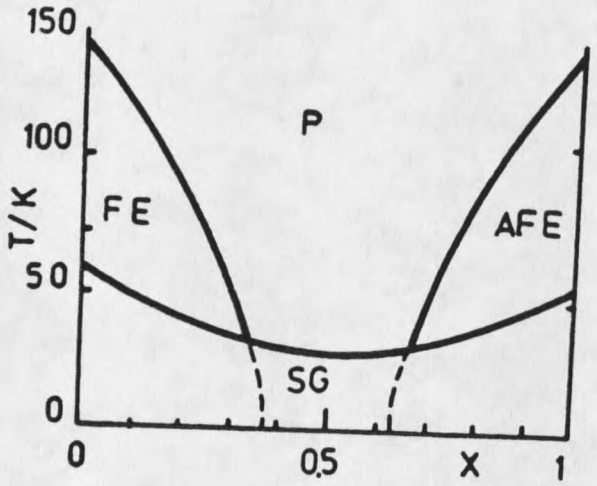

Figure 12. Calculated phase diagram for RADP showing the stability limits of the paraelectric phase with respect to a freezing into the ferro-, antiferroelectric and proton glass phases.

and $J_o^{ADP}=-J_o^{RDP}$. Also, assume that the couplings between the ADP and RDP sites are zero. The transition temperatures for this example can be obtained from Eq.(4.8) and Eq.(4.11). These results are plotted in Fig. 12. For the concentration x=0.35 a glass transition temperature T_g about 30 K is obtained in agreement with experiment, but T_c is only a little bit lower. The calculated phase diagram predicts a concentration range $0.35<x<0.65$ where a glass transition occurs in comparison to experimental results that show glass transitions for $0.20<x<0.80$.

CHAPTER 5

RESULTS AND DISCUSSION

This chapter covers the experimental results of this work in four sections and a discussion of these results. The first three sections include results from bulk measurements i.e. dielectric, spontaneous polarization and field-cooling experiments and the fourth contains results at the atomic level i.e. nuclear magnetic resonance. The experimental setup for each of these experiments is given in Chapter 3.

Dielectric Measurements

Dielectric measurements have been performed in both the deuterated and undeuterated proton glass rubidium ammonium dihydrogen arsenate ($Rb_{1-x}(NH_4)H_2AsO_4$) along the tetragonal a axis. Ammonium concentrations (x) of 0, 0.01, 0.05, 0.10 and 0.40 were studied for the undeuterated sample (RADA) while ammonium concentrations of 0, 0.05, 0.10 and 0.28 were studied for the deuterated counterpart (DRADA).

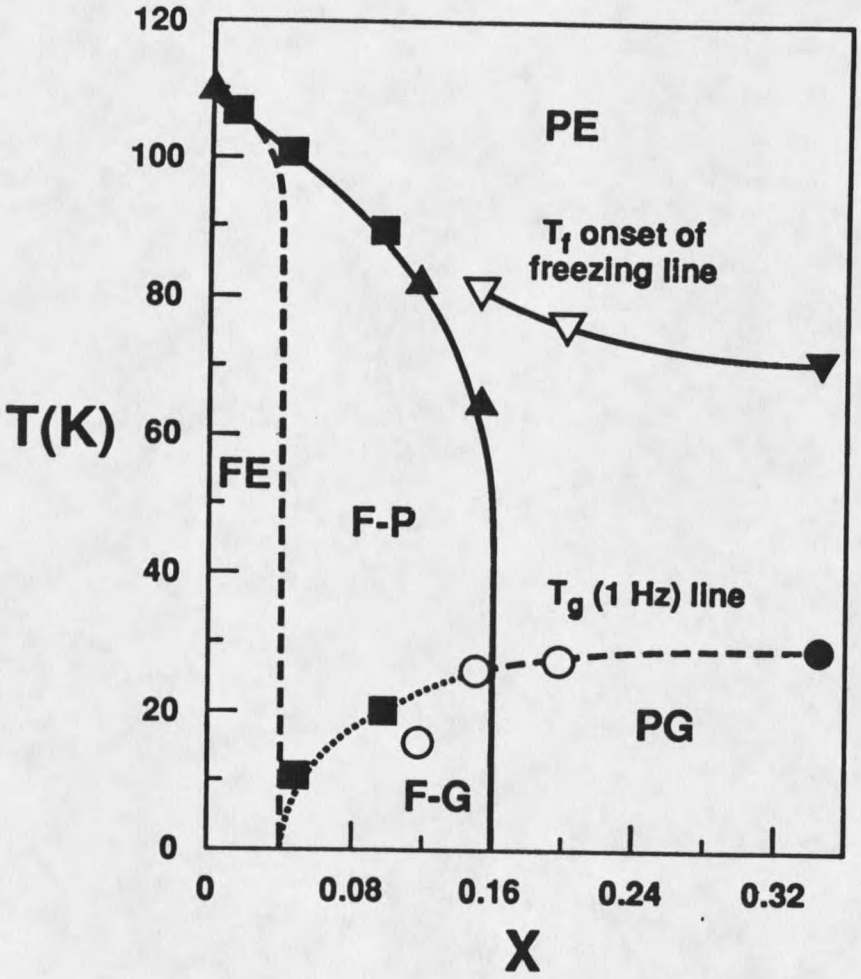

Figure 13. The partial phase diagram of RADA as a function of fractional ammonium concentration x and temperature T. PE, FE, PG, F-P and F-G denote paraelectric and ferroelectric phases, proton glass regime, mixed ferroelectric-paraelectric and ferroelectric-proton glass phases respectively. The dotted line represents extension from this work. The solid squares represent data from this work; other symbols represent data from Trybula et al. (Ref. 9)

These measurements are a continuation of the work started by Z. Trybula who first observed[9] coexistence in the arsenates. Our results extend his measurements to lower ammonium concentrations and suggest a change in the phase diagram for the undeuterated arsenates published in Ref. 9. This suggested phase diagram is shown in Fig. 13 where the dotted line is drawn to indicate that the coexistence region extends down to lower ammonium concentrations. Coexistence may be present down to extremely small ammonium concentrations, however, dielectric measurements could not detect such a phase down to x=0.01 in the undeuterated samples.

Fig. 14 shows the temperature dependence of the real part of the dielectric constant ε_a' for various values of ammonium concentration x for the undeuterated sample. Fig. 15 represents the same but for the deuterated counterpart. Both these Figures represent data taken at 1 kHz. For certain x values there are two transitions as evident from the graphs. The first transition (T_c) on lowering the temperature corresponds to the ferroelectric transition and the second "transition" (T_g) at still lower temperatures is the proton glass transition. This "transition" temperature is frequency dependent and is defined as the temperature at which ε_a' begins to drop more rapidly with decreasing temperature for that frequency.

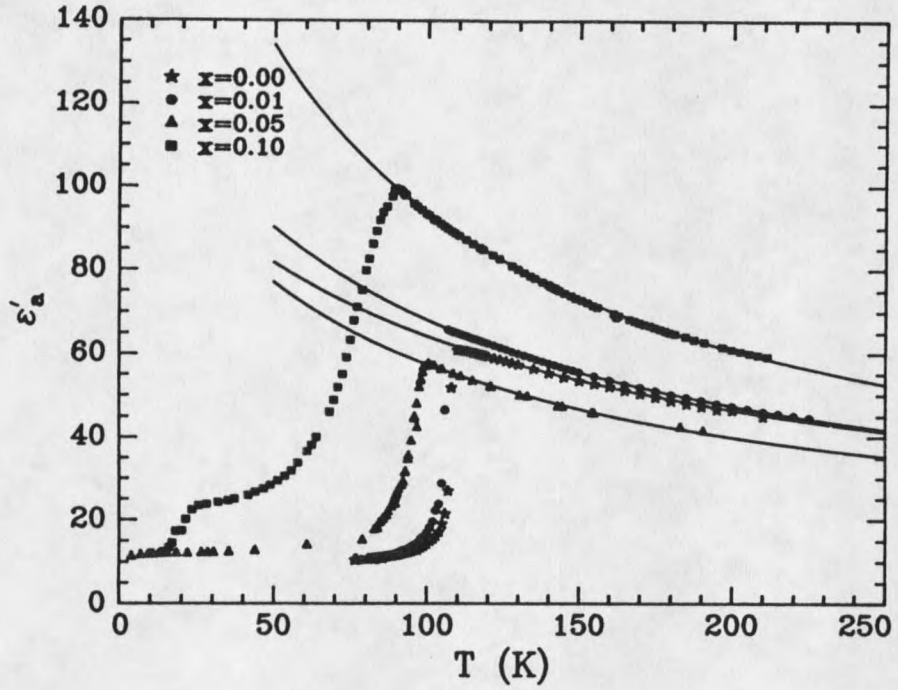

Figure 14. Temperature dependence of the real part of the dielectric constant ε_a' measured along the a axis for various ammonium concentrations x in RADA. Solid line represents a fit to Eq.(5.1); see Table 1 for fitting constants.

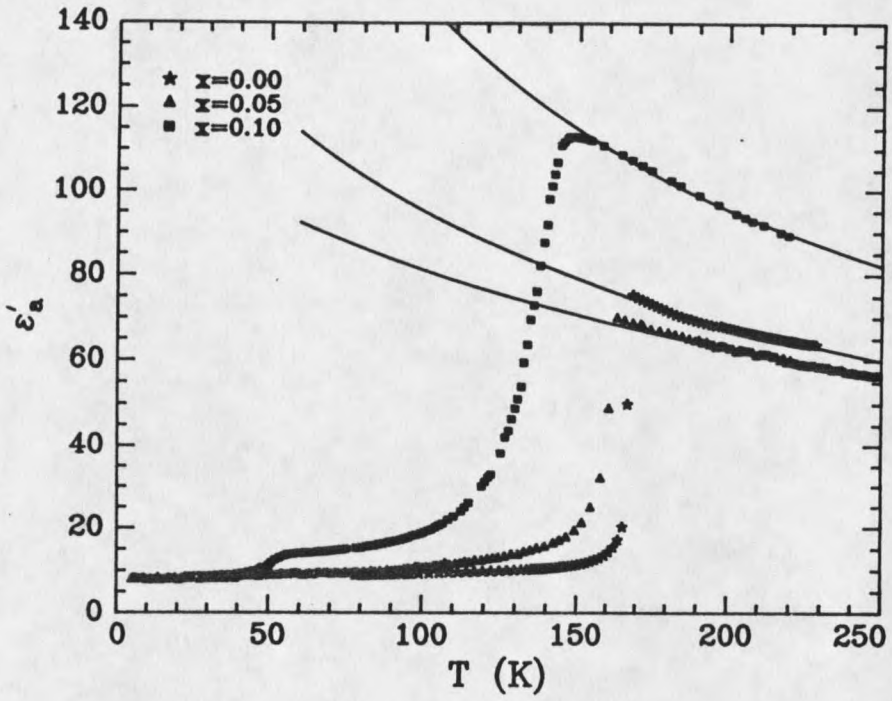

Figure 15. Temperature dependence of the real part of the dielectric constant ε_a' measured along the a axis for various ammonium concentrations x in DRADA. Solid line represents a fit to Eq.(5.1); see Table 1 for fitting constants.

Table 1: Tabulated temperatures of various transitions mentioned in the text including the activation energies responsible for dielectric relaxation. These results (except for the activation energy) are obtained by analyzing the data taken at 1 kHz.

	UNDEUTERATED						DEUTERATED					
X	T_c(K)	T_g(K)	$\varepsilon'_{a\infty}$	C (K)	T_o(K)	E_a(meV)	T_c(K)	T_g(K)	$\varepsilon'_{a\infty}$	C (K)	T_o(K)	E_a(meV)
0	110	—	10	11100±100	-105±2	—	168	—	7	19800±300	-125±5	—
0.01	107	—	10	10500±100	-81±1	—	—	—	—	—	—	—
0.05	101	15	10	8100±200	-71±3	—	163	56	7	22500±400	-204±7	99
0.1	90	21	10	12900±100	-54±1	59	146	57	7	24700±400	-79±4	104
0.28								50				75
0.40		40				200						

Table 1 summarizes the transition temperatures for various x values at 1 kHz. In the RADA sample for x=0.01, the dielectric constant ε_a' falls to 9 below T_c. This is also the value for ε_a' for the pure (x=0) sample below T_c, thus ruling out the possibility of observing a glass transition. We suggest that a more sensitive technique like nuclear magnetic resonance or electron paramagnetic resonance be used to detect proton glass behavior. The sharper drop in ε_a' below T_c for decreasing x is consistent with the almost vertical drop one expects to observe in the pure RDA crystal which undergoes a first order transition[22,23] at T_c.

Interesting effects are observed upon deuteration. The transition temperatures are significantly increased as can be seen in Table 1 by comparing the transition temperatures of the deuterated and undeuterated samples with similar x values. These results reflect the greater asymmetry[24] in the O-D...O bond, a quantum-mechanical effect due to the larger mass of the deuteron as compared to the proton. The value of ε_a' at T_c is higher in the deuterated samples. We note that T_c for DRADA x=0.05 is closer to that for x=0 unlike in the RADA case where T_c for x=0.05 is halfway between that of x=0 and x=0.10. This could be attributed to the uncertainty in x and the lesser deuteration content due to repeated redissolving of the solute in heavy water which was done to obtain good crystals. From Figs. 16 to 19, we

see that in the case of the deuterated samples at low temperature ε_a'' goes to zero well above zero K, while for the undeuterated crystals it stays above zero, in some cases approaching zero with finite slope as temperature goes to zero. A possible explanation is that the heavier deuteron is more localized in its bond and freezes in at low temperatures resulting in negligible lossy behavior while in the undeuterated case the freezing temperature would have to be substantially lower to get a similar effect.

The dielectric constant ε_a' from T_o up towards higher temperatures is found to obey the Curie-Weiss behavior. The solid lines in Figs. 14 and 15 represent fits to the Curie-Weiss formula:

$$\varepsilon_a' - \varepsilon_{a\infty}' = C/(T - T_o) \qquad (5.1)$$

where $\varepsilon_{a\infty}'$ is the "infinite frequency" dielectric response, C is the Curie-Weiss constant and T_o is the Curie-Weiss temperature. Table 1 shows these fitting parameters for various concentrations x, where the $\varepsilon_{a\infty}'$ value is the average of those obtained from Figs. 14, 15, 20 and 21. A similar fit was made[25] in a RADP sample along the a axis close to the antiferroelectric boundary of the phase diagram. Nagamiya[26] has also made Curie-Weiss fits along

the a and c axes in ADP with negative Curie-Weiss temperatures. It is still unclear why in the case of our samples which have a ferroelectric transition we get a negative Curie-Weiss temperature. One possibility is that even though the crystal is ferroelectric along c it may have a tendency to align antiferroelectrically along a. Essential features of the proton-glass behavior are shown in Figs. 16 to 19. Such behavior at low temperatures is typical for proton glasses in that it shows a dispersion and characteristic maxima of $\varepsilon_a''(T)$ a few degrees below the glass transition temperature T_g. The dispersion is greater in the x=0.10 samples as compared to the x=0.05 samples. This must be true since the ammonium concentration is higher. We point out that the variation in ε_a'' in the x=0.05 sample Fig. 16(a) is much lower in the undeuterated crystal as compared to the deuterated one shown in Fig. 17(a).

In an attempt to analyze the dielectric relaxation mechanisms below T_g we have constructed Cole-Cole plots Figs. 20 and 21, for the x=0.10 sample from the data shown in Figs. 18 and 19. Both plots show that the relaxation processes cannot be characterized by a single relaxation time. This spread in relaxation times results from the fractal nature of the effective potential in which $HAsO_4$ and H_3AsO_4 groups in effect diffuse by means of intrabond proton transfer.[27,28] This diffusion is responsible for the

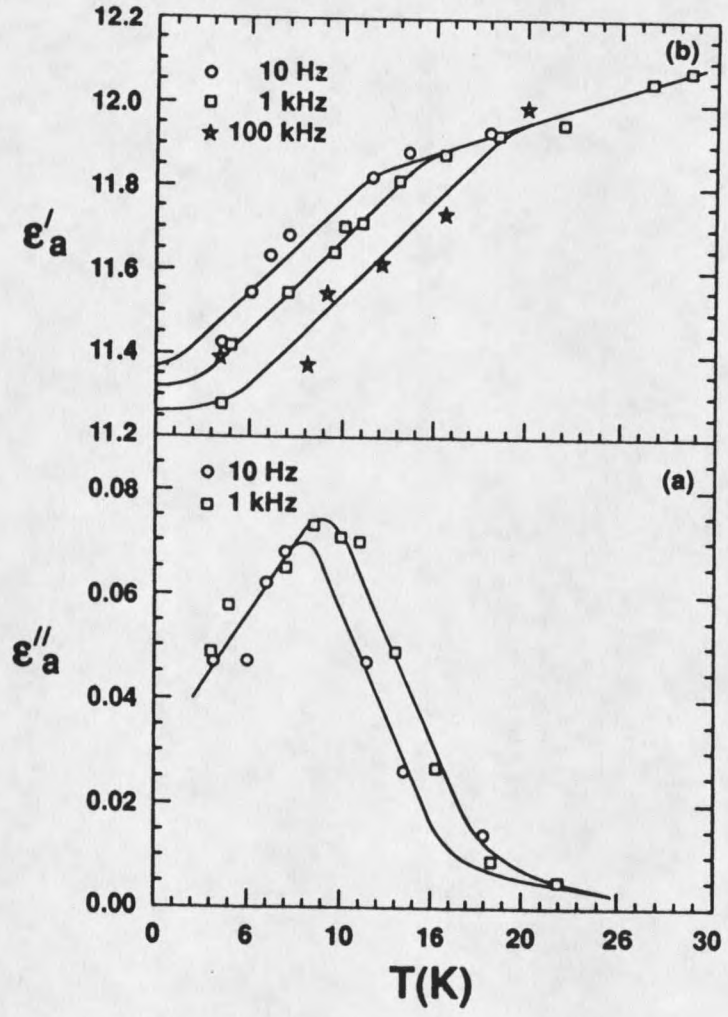

Figure 16. Temperature dependence of the (a) imaginary part ε_a'' and (b) real part ε_a' of the dielectric permittivity in the proton glass regime for x=0.05 RADA. Solid lines are guides to the eye.

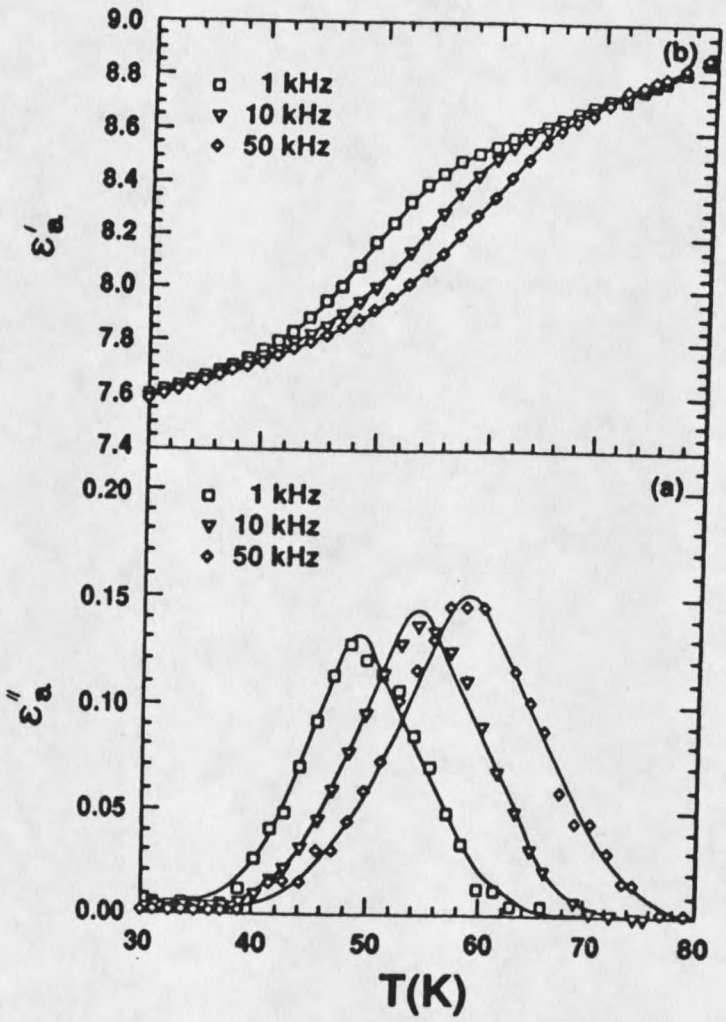

Figure 17. Temperature dependence of the (a) imaginary part ε_a'' and (b) real part ε_a' of the dielectric permittivity in the proton glass regime for x=0.05 DRADA. Solid lines are guides to the eye.

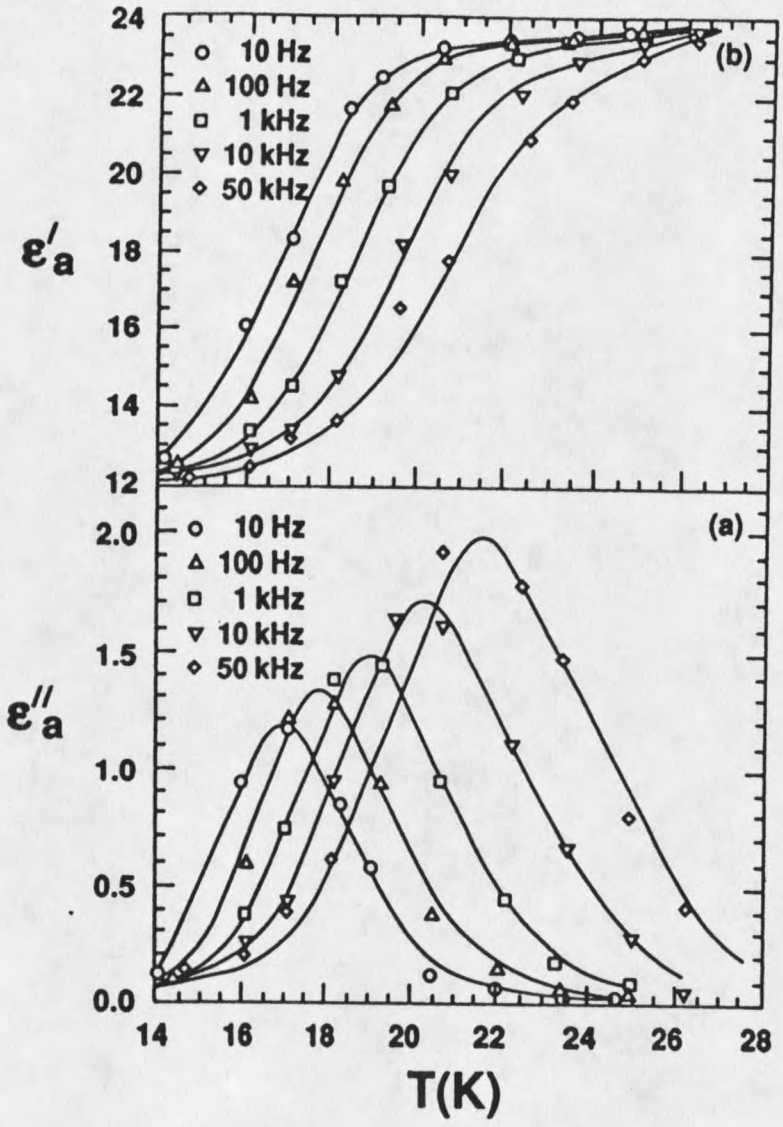

Figure 18. Temperature dependence of the (a) imaginary part ε_a'' and (b) real part ε_a' of the dielectric permittivity in the proton glass regime for x=0.10 RADA. Solid lines are guides to the eye.

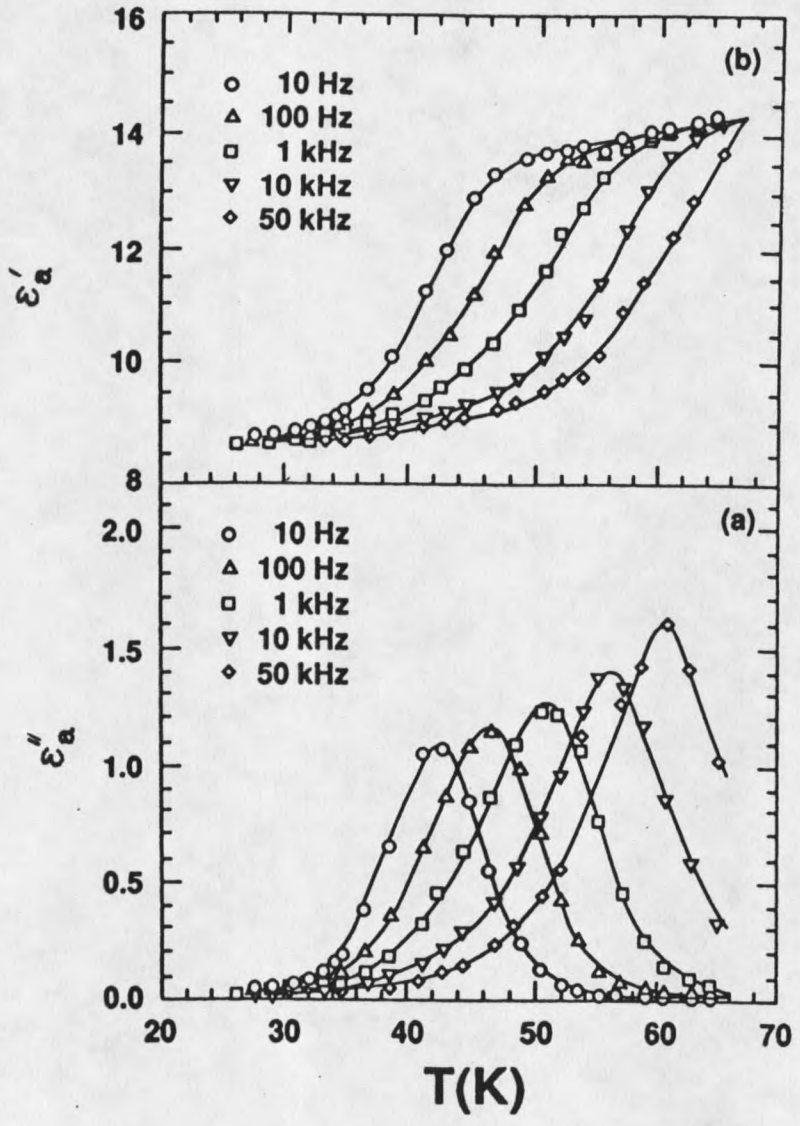

Figure 19. Temperature dependence of the (a) imaginary part ε_a'' and (b) real part ε_a' of the dielectric permittivity in the proton glass regime for x=0.10 DRADA. Solid lines are guides to the eye.

dielectric relaxation. As these groups cross potential barriers, the associated set of proton intrabond transfers can be called a cluster of pseudospins flips, in analogy with spin glass behavior. Similar spreads in relaxation times have been seen in spin glasses[29] where flipping of clusters of spins is the primary relaxation mechanism. As temperature decreases below T_g there is a gradual increase in the distribution of relaxation times as is evident from the Cole-Cole plots in Figs. 20 and 21. A similar result was observed by Kutnjak et al.[30] in DRADA with x=0.25 for the c-axis permittivity where they have used a Fröhlich-type distribution to analyze their dielectric results. For this ammonium concentration there is no ferroelectric transition. The distribution of relaxation times is greater in the undeuterated sample as can be seen from Figs. 20 and 21. To get the same shape for DRADA as for RADA we have to go to about twice the temperature, just as to get to T_c in the pure crystal we have to go to about twice as high a temperature. For a system with a single relaxation time the Cole-Cole plot would be a semicircle with its center on the ε_a' axis. The lowest-temperature plots in Fig. 20 probably deviates at the right-hand end from the circular shape shown, because it is unlikely that the maximum ε_a' would suddenly increase at the lowest temperature.

Assuming that the temperatures corresponding to the

peaks in $\varepsilon_a''(T)$ in Figs. 16(a) to 19(a) obey the exponential Arrhenius law

$$f=f_o\exp(E_a/kT) \qquad (5.2)$$

where f is the frequency, f_o is the attempt frequency and E_a is the activation energy, our results for the activation energy are summarized in Table 1 for x=0.10 and x=0.05 (DRADA). The activation energy is greater in the case of the deuterated sample by almost a factor of 2. Here, $2E_a$ is approximately the energy required to create an $HAsO_4$-H_3AsO_4 pair from two H_2AsO_4 groups. Fig. 13 shows the phase diagram for the undeuterated RADA family of proton glasses including data points from Ref. 9. Data points for the 1 Hz T_g line in Fig. 13 have been obtained by extrapolating to 1 Hz in Figs. 16(b) and 18(b) for x=0.05 and x=0.10 respectively.

In order to compare the dielectric response of the deuterated and undeuterated crystals with ammonium concentrations that show coexistence of proton glass and ferroelectric order, measurements were made on crystals with larger ammonium concentrations that show pure proton glass behavior. Here we see that the ferroelectric transition is suppressed and the glass transition occurs at higher temperatures. This glass transition is seen to be

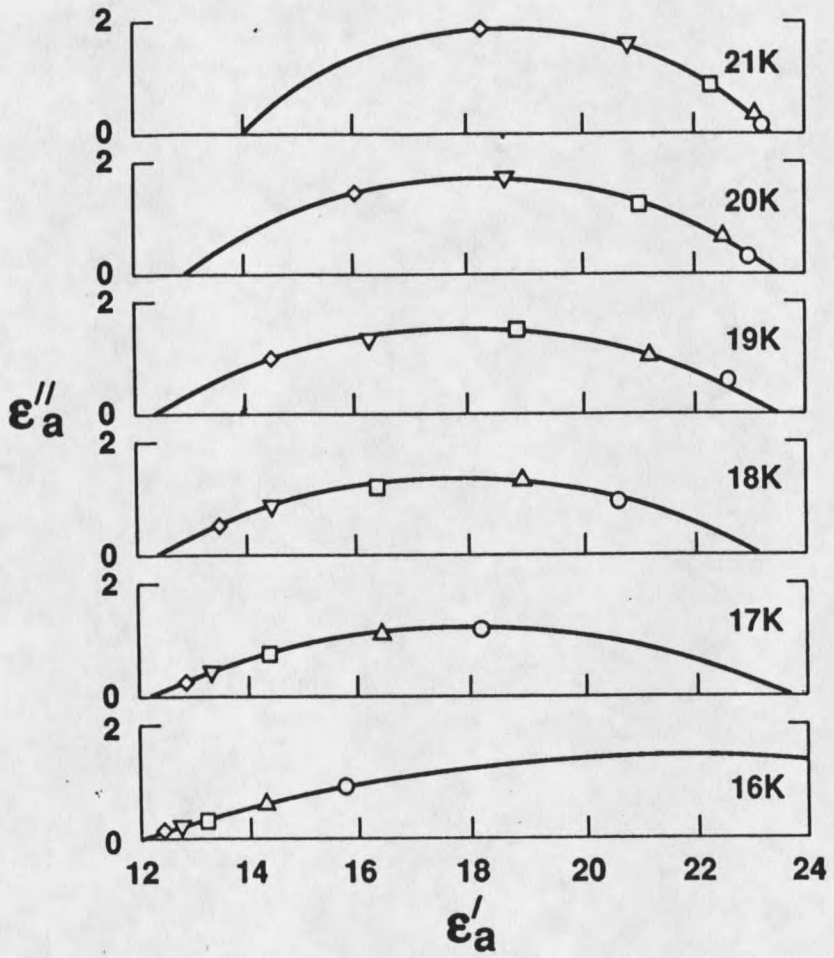

Figure 20. Cole-Cole plots for x=0.10 RADA in the proton glass region. The symbols represent the same frequencies as in Figs. 18 and 19. Solid lines represents fits to the equation of a circle.

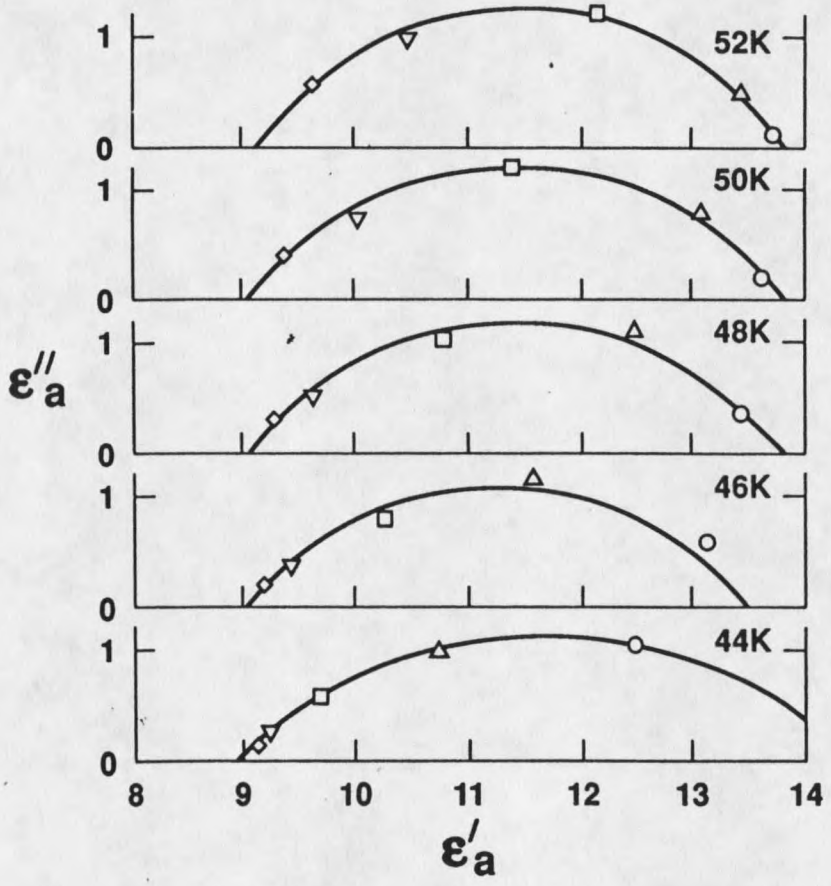

Figure 21. Cole-Cole plots for x=0.10 DRADA in the proton glass region. The symbols represent the same frequencies as in Figs. 18 and 19. Solid lines represents fits to the equation of a circle.

smeared out when compared to the ferroelectric transition temperatures in Fig. 14 and 15. This smearing effect is due to the presence of internal random fields[16] and is much more prominent in the undeuterated sample. This is seen in the dielectric measurements in Figure 22 for the undeuterated RADA with x=0.4 and Figure 23 for the deuterated RADA sample with x=0.28. The activation energies for dielectric relaxation are calculated from Eq.(5.2) and are tabulated in Table 1. We see that the activation energy for the undeuterated sample (200 meV) is higher when compared to samples with lesser ammonium content. However if one were to divide the data in Fig. 22(b) with the fraction of the sample that remains paraelectric at each temperature, it would move the peaks in Fig. 22(b) slightly to the left, and upwards by increasing the amounts for peaks occurring at lower temperatures. This would result in the locus of the peaks having a smaller slope and consequently a smaller activation energy. Dielectric measurements were also performed along the c axis in the case of the x=0.28 deuterated crystal. These results are shown in Figure 24. In the absence of a ferroelectric transition, from Figures 23 and 24 we see that the values of ε' and ε'' are found to be greater along the a axis as compared to the c axis.

Figures 14 and 15 show that there exists a coexistence

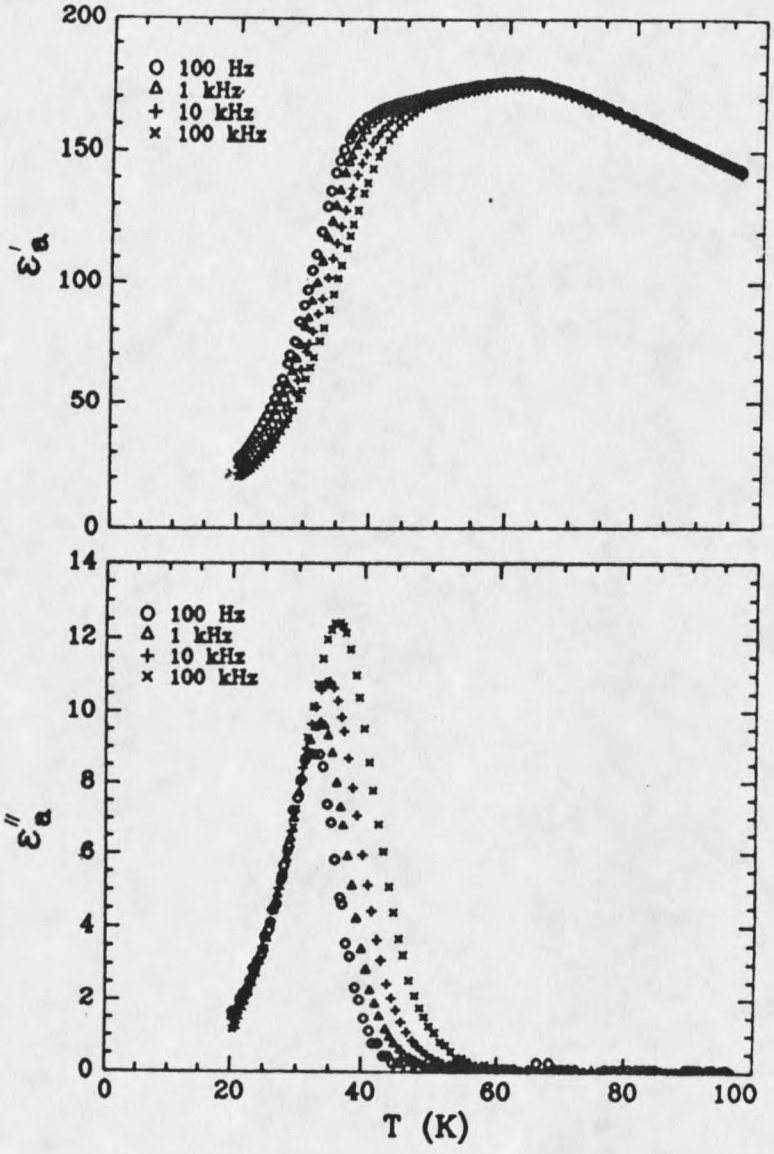

Figure 22. Temperature dependence of the (a) real part ε_a' and (b) imaginary part ε_a'' of the dielectric permittivity measured along the a axis in the proton glass regime for x=0.40 RADA.

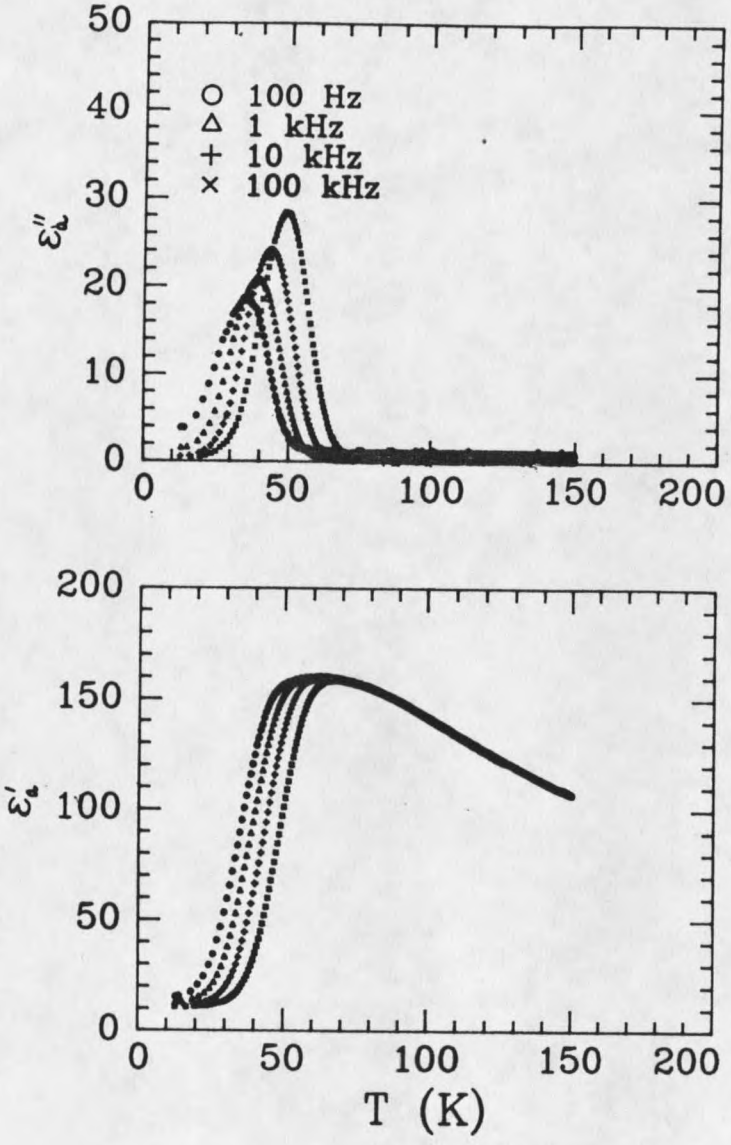

Figure 23. Temperature dependence of the (a) real part ε_a' and (b) imaginary part ε_a'' of the dielectric permittivity measured along the a axis in the proton glass regime for x=0.28 DRADA.

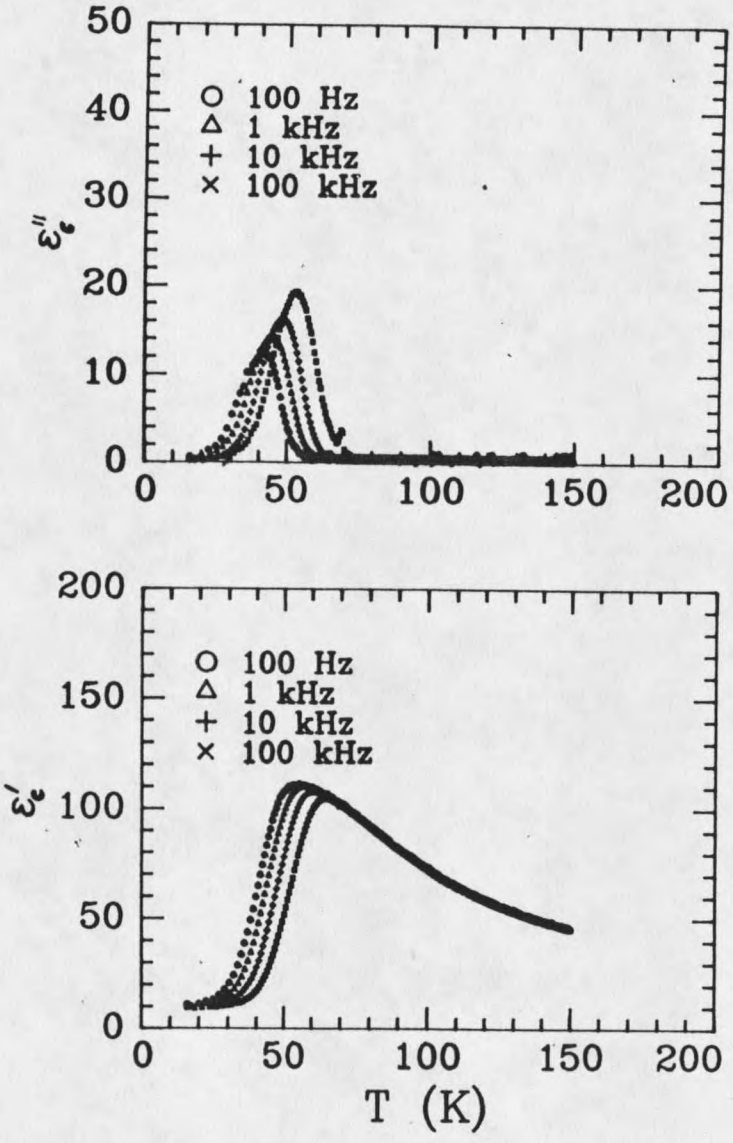

Figure 24. Temperature dependence of the (a) real part ε_a' and (b) imaginary part ε_a'' of the dielectric permittivity measured along the c axis in the proton glass regime for x=0.28 DRADA.

of ferroelectric and proton glass phases below T_g. We believe that these mixed crystals with x=0.10 and 0.05 have ferroelectric clusters intimately interlocked with proton glass clusters below T_g. The measurement of the spontaneous polarization confirms this claim as we see that the maximum value of the spontaneous polarization in the mixed crystals is smaller when compared to that for the pure ferroelectric.

Spontaneous Polarization Measurements

Spontaneous polarization of mixed single crystals of RADA and DRADA are presented together with the pure ferroelectric RDA and DRDA. These measurements were done using a Sawyer-Tower bridge as explained in Chapter 3. There is a sharp rise in the spontaneous polarization at the ferroelectric transition temperature T_c for the pure crystals as this transition is first order. The change in the spontaneous polarization in the mixed crystals is gradual, however, indicating the presence of acid hydrogens and ammonium cations that are still mobile and in the paraelectric phase.

Figure 25 shows the spontaneous polarization of the undeuterated RADA sample. The ferroelectric transition for x=0 is first order and the transition temperature T_c is

found to be 110 K. This is evidenced by the sharp rise in spontaneous polarization at T_c. The spontaneous polarization reaches a value of (3.6±0.5) μCcm^{-2} at temperatures far below T_c. The large error bars in the spontaneous polarization results from the uncertainty in computing the surface area of the sample due to its small size. Within the limits of our experimental error this value agrees with that reported by Kamysheva et al.[22] who have obtained a maximum value of (4.2±0.2) μCcm^{-2} from specific heat measurements.

From the expression of the free energy (G) as a function of polarization (P):

$$G(P,T) = G_o(T) + \frac{\alpha}{2}P^2 + \frac{\beta}{4}P^4 + \frac{\gamma}{6}P^6 + \ldots \qquad (5.3)$$

where $\alpha = \alpha_o(T-T_o) = 4\pi(T-T_o)/C$, C is the Curie-Weiss constant and T_o is the Curie-Weiss temperature, we have calculated the thermodynamic coefficients β and γ for the pure crystals. In Fig. 26 we show the dielectric constant as a function of temperature measured along the c axis at 1 kHz and very low applied electric field (10 V/cm) for the pure crystals. The solid line is a fit to the Curie-Weiss law of Eq.(5.1) along the c axis. This fit gives a value of

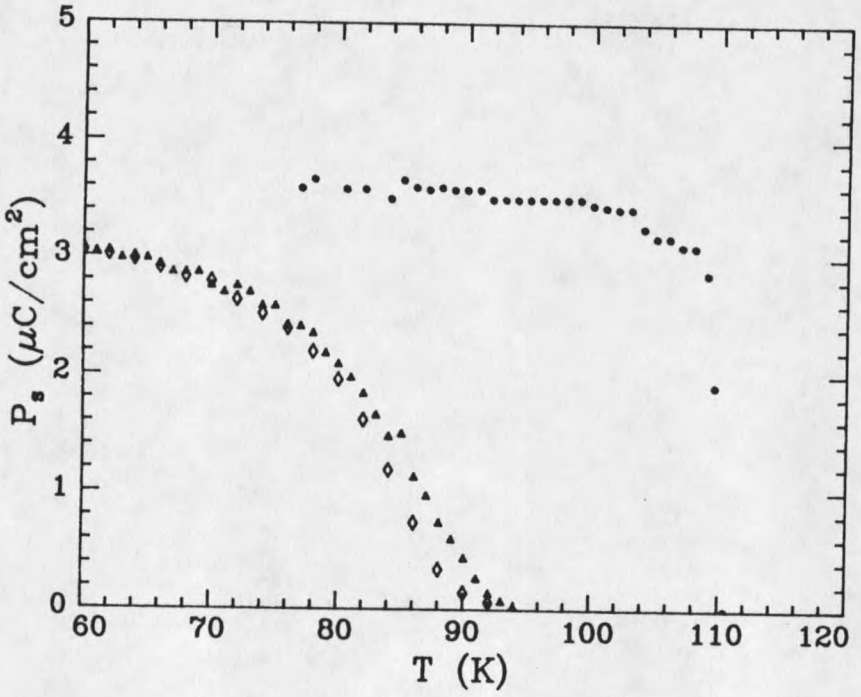

Figure 25. Spontaneous polarization obtained from saturated hysteresis loops in RDA (x=0; •) and RADA (x=0.08; ▲) as a function of temperature. The open diamond symbol represents spontaneous polarization obtained from Eq. (5.4) and Fig. 27 for RADA x=0.08.

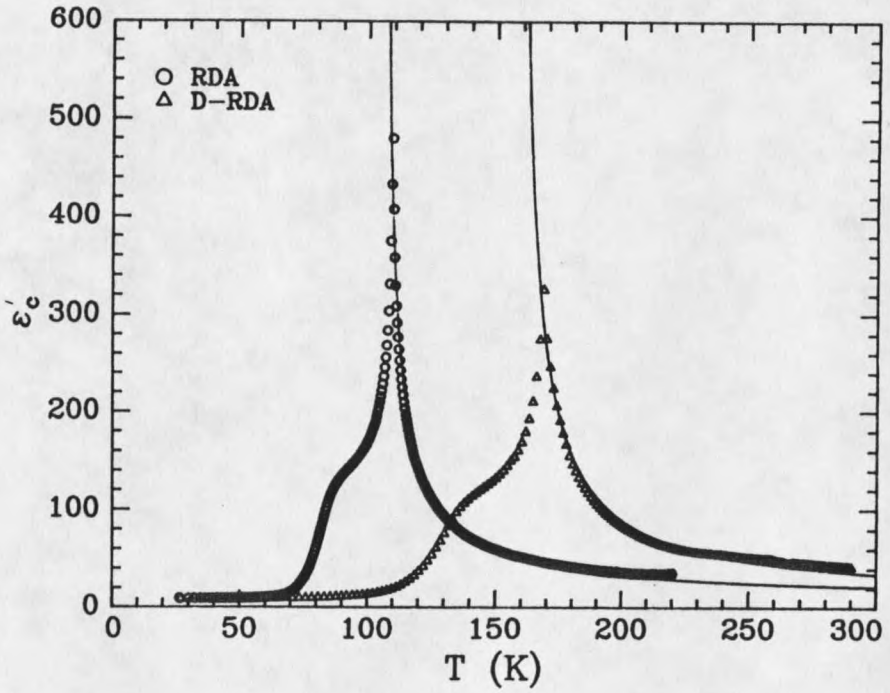

Figure 26. Real part of the dielectric permittivity ε_c' at 1 kHz as a function of temperature along the c axis, (O) for RDA and (Δ) for DRDA. Solid line represents a fit to the Curie-Weiss law of Eq. (5.1).

C=2200±20 K and T_o=104 K for RDA; we have assumed a value of 10 for the "infinite frequency" dielectric response ε_∞. Using this value for C we calculate β=-16.7x10^{-10} c.g.s. and γ=15.4x10^{-18} c.g.s. from the expression $(\Delta P_s)^2$=-3β/4γ and $(\Delta P_s)^2$=-4α/β where ΔP_s=3.0 μCcm^{-2} is the jump in the spontaneous polarization at T_o. It must be pointed out that Eq.(5.3) truncated at the P^6 term cannot be expected to fit such a big P_s [$\Delta P_s \approx P_s$(0 K)] very well. Table 2 shows the corresponding values obtained from saturated hysteresis loops[31] and from specific heat measurements[22]. The difference in our values arises from the low T_o and C values obtained from fitting Eq.(5.1) to Fig. 26.

Table 2. Tabulated values of ß and γ defined in Eq.(5.3) for RDA and DRDA together with parameters defined in the text.

Ref.	Sample	C(K)	T_o(K)	ΔP_s μC.cm^{-2}	ß c.g.s.	γ c.g.s.
31	RDA	-	108.5	3.7	-20x10^{-11}	12x10^{-19}
22	RDA	3100	108.5	3.6	-6.9x10^{-11}	4.4x10^{-19}
This work	RDA	2200	104.0	3.0	-16.7x10^{-10}	15.4x10^{-18}
This work	DRDA	3500	156.0	4.5	-9.4x10^{-10}	3.8x10^{-18}

The spontaneous polarization for x=0.08 RADA is also shown in Fig. 25, and can be compared to that for the pure ferroelectric. The spontaneous polarization rises gradually

in this case due to the presence of the ammonium cation centers, many of which are still in the paraelectric phase for some temperature range below T_c. However, at temperatures below 55 K the applied electric field needed to obtain saturated hysteresis loops exceeds the dielectric breakdown field of the sample, hence saturation polarization could not be computed below this temperature. The value of the spontaneous polarization measured at the lowest temperature reported is (3.0±0.5) μCcm^{-2}. We note that this value of the saturation polarization is less than that for the pure sample. We also performed dielectric measurements along the a axis for the same mixed crystal to verify the variation in spontaneous polarization obtained from hysteresis loops as a function of temperature below T_c. The glass transition is not seen in this sample at the temperatures covered in this experiment but is seen at lower temperatures (see Figure 14). The spontaneous polarization in this case can be obtained from:

$$P_{sd}=P_{so}\left(\frac{\epsilon_1'}{\epsilon_1'+\epsilon_2'}\right) \qquad (5.4)$$

where P_{sd} is the spontaneous polarization obtained from the dielectric data, P_{so} is the maximum spontaneous polarization

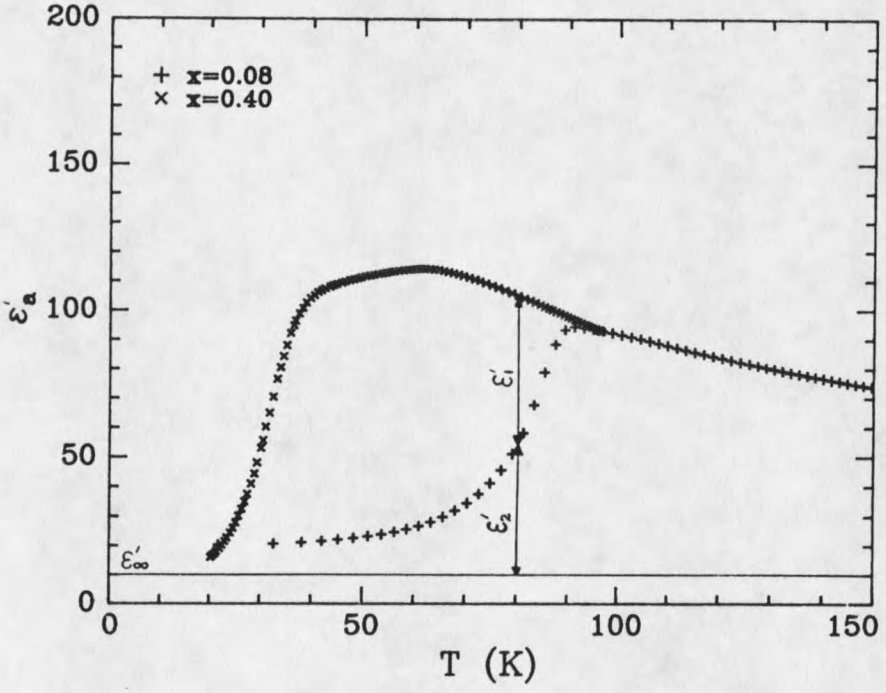

Figure 27. Real part of the dielectric permittivity ε_a' for the undeuterated mixed crystals at 1 kHz as a function of temperature along the a axis. ε_∞' is assumed to be 10.

of the pure crystal well below T_c, and ε_1' and ε_2' are defined in Fig. 27. Here ε_2' represents the contribution to the dielectric constant from the paraelectric portion of the x=0.08 sample and $(\varepsilon_1'+\varepsilon_2')$ would represent the contribution to the dielectric constant from the same sample in the absence of the ferroelectric phase transition. Dielectric data for RADA x=0.4 has been included to help extrapolate qualitatively the Curie-Weiss behavior in the x=0.08 crystal to temperatures below T_c. In Fig. 25 we show the variation in P_{sd} as a function of temperature below T_c and compare it to that obtained for the same sample from saturated hysteresis loops. The agreement is good within the limits of experimental error. Here we have used P_{so}=3.6 μCcm^{-2} from Fig. 25.

In the case of mixed RADP samples, however, the spontaneous polarization is found to approach the value of the pure ferroelectric RDP[32] at low temperatures. It must be pointed out that coexistence of ferroelectric and proton glass phase has not been reported in RADP mixed crystals below the ferroelectric transition temperature.

Fig. 28 shows the spontaneous polarization in the case of the deuterated samples. Here, deuteration effects raise the transition temperatures and the values of the spontaneous polarization as compared to the undeuterated counterpart. Similar effects of deuteration are seen in the

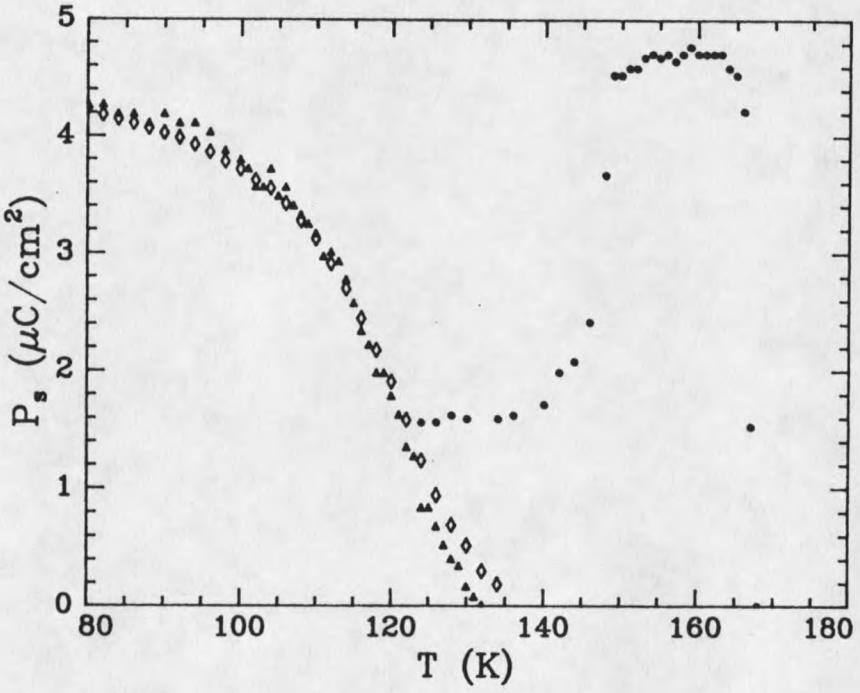

Figure 28. Spontaneous polarization obtained from saturated hysteresis loops in DRDA (x=0; •) and DRADA (x=0.08; ▲) as a function of temperature. The open diamond symbol represents spontaneous polarization obtained from Eq. (5.4) and Fig. 29 for DRADA x=0.08.

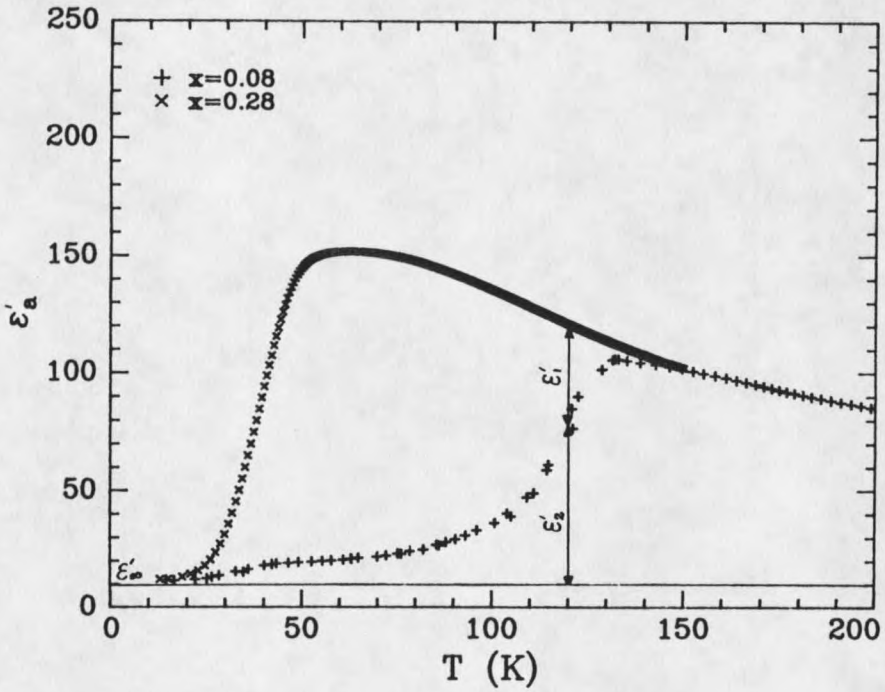

Figure 29. Real part of the dielectric permittivity ε_a' for the deuterated mixed crystals at 1 kHz as a function of temperature along the a axis. ε_∞' is assumed to be 10.

phosphates.[33,34] The transition in the pure sample is sharp when compared to the mixed sample. The value of the spontaneous polarization below T_c for the pure sample is (4.7±0.2) μCcm^{-2}. The variation in the spontaneous polarization in the x=0.08 sample is gradual as in the case of the undeuterated sample and approaches a value of (4.2±0.2) μCcm^{-2} at the lowest temperatures measured. From Fig. 26, the Curie-Weiss fit for DRDA yields C=3500±50 K and T_c=156 K. T_c for DRDA is found to be 168 K. This increase of about 1000 K for the Curie-Weiss constant in the deuterated sample is consistent with that observed in RDP[34] and KDP[35] upon deuteration. Using this value for C we obtain for DRDA, $\beta=-9.4\times10^{-10}$ c.g.s. and $\gamma=3.8\times10^{-18}$ c.g.s. where we have used ΔP_s=4.5 μCcm^{-2} as the jump in the spontaneous polarization at T_c. These values are tabulated in Table 2. We have calculated P_{sd} for the deuterated case from Fig. 29 and Eq.(5.4) by a method analogous to that used to calculate the spontaneous polarization from the dielectric data in the undeuterated crystals. From Fig. 28 we have used P_{so}=4.7 μCcm^{-2}. In Fig. 29 the glass transition for the x=0.08 crystal is seen around 43 K where the dielectric constant begins dropping faster with decreasing temperature. Here too, dielectric data for x=0.28 have been included to help extrapolate the Curie-Weiss behavior of the x=0.08 crystal below T_c. The result is plotted in Fig.

28 and can be compared to that obtained for the same sample from saturated hysteresis loops.

In Fig. 28 we notice a drop in the spontaneous polarization for the pure sample below 153 K. This effect was seen in two separate samples. Below 120 K the hysteresis loops could not be saturated because the necessary electric field would exceed the dielectric breakdown field of the crystal. However, saturated loops appeared above 120 K with increasing polarization as temperature was increased. This effect could indicate pinning of ferroelectric domains due to crystal defects or impurities at lower temperatures, thus giving a reduced value of spontaneous polarization. Further investigation of this effect is planned.

The experimental results show that deuteration increases the maximum value of the spontaneous polarization in the pure crystals. Also, the maximum value of the spontaneous polarization in the mixed crystals is lower than that of the pure crystal. This indicates that at the lowest temperatures recorded there are still paraelectric clusters intimately interlocked with the ferroelectric clusters. The gradual increase in spontaneous polarization below T_c in the mixed crystals follows the gradual decrease in the dielectric constant of the corresponding crystals below this temperature.

Field Cooling Measurements

Static polarization measurements have been performed in DRADA with x=0.28. A crystal with this ammonium concentration has no ferroelectric or antiferroelectric transition but only a "glass transition". This can be seen in the dielectric measurements shown in Fig. 23. The spontaneous polarization in these crystals is zero. A polarization can be generated however, by cooling the crystal in the presence of an external electric field. This polarization is called "remanent" and is the polarization obtained when the external field is turned off. In the case of magnetic spin glasses it is common to perform field-cooling experiments to determine the magnetic susceptibility. In contrast to magnetic spin glasses where one has random bond interactions, proton glasses are characterized by the presence of both random bonds and random fields.[16] This difference is due to the fact that the magnetic spins are essentially uncoupled from the lattice, whereas the O-D...O bonds are part of the crystal lattice and are thus strongly affected by substitutional disorder. Because of the presence of this random dc bias in proton glasses, the response of such systems below the ergodic limit to an external electric field would depend on the history of the system, i.e. how the low temperature

phase was reached. If the system is cooled in zero field and then the field is turned on, the corresponding zero-field-cooled susceptibility χ_{ZFC} would differ from the field-cooled susceptibility χ_{FC} obtained by cooling the sample in the presence of an external field.

Static polarization measurements were carried out along the a tetragonal axis at two heating and cooling rates and the results are found to depend on these rates of temperature changes. This experiment is an extension of the work done by Levstik et al.[36] on a deuterated phosphate glass to arsenate glasses. Upon cooling into the glass state each acid deuteron freezes at random into one of the two O-D...O bond sites. The position of the acid deuteron within the bond is influenced by the presence of the ND_4 groups, which are placed nonsymmetrically with respect to the surrounding cations. This tilts the double well potential barrier thus inducing a random effective local electric field as mentioned in Chapter 4.

The "glass transition" temperature at the lowest frequency of 100 Hz is ≈5.0 K as can be seen in Fig. 23. Figures 30 and 31 show the temperature dependence of the field-cooled and zero-field-cooled static polarization of a DRADA x=0.28 crystal along the a axis for different heating and cooling rates. The crystal was first cooled in zero field to about 8 K, then a dc field of 500 V/cm was

turned on. The corresponding zero-field-cooled susceptibility $\chi_{ZFC}=\lim_{E\to 0}P(E,T)/\varepsilon_o E$ is then computed knowing the charge stored in the crystal. The sample is then heated through the "glass transition" and cooled with the field left on. The corresponding field-cooled susceptibility $\chi_{FC}=P(E,T)/\varepsilon_o E$ is calculated likewise. The field is then turned off and a remanent polarization is observed which decays as a function of heating rate and temperature. Static susceptibility measurements corresponding to these various stages is seen in Figures 30 and 31.

The initial response upon turning the field on is the "infinite frequency" dielectric response due to the sudden application of the applied field. This arises from the electronic and direct ionic response to switching the electric field on and off. A similar effect is seen upon turning the field off.

We distinguish, in Figures 30 and 31, three regions of interest that yield different responses to the application of an electric field. The paraelectric phase above 60 K is monodispersive as the deuterons are mobile enough to follow the exciting electric field even at high frequencies. The monodispersive nature can be seen in Fig. 23. Below 20 K the system is nonergodic as the deuterons are frozen in their bond sites. From 20 K to about 60 K, thermal motion allows for the acid deuterons to move within their bonds.

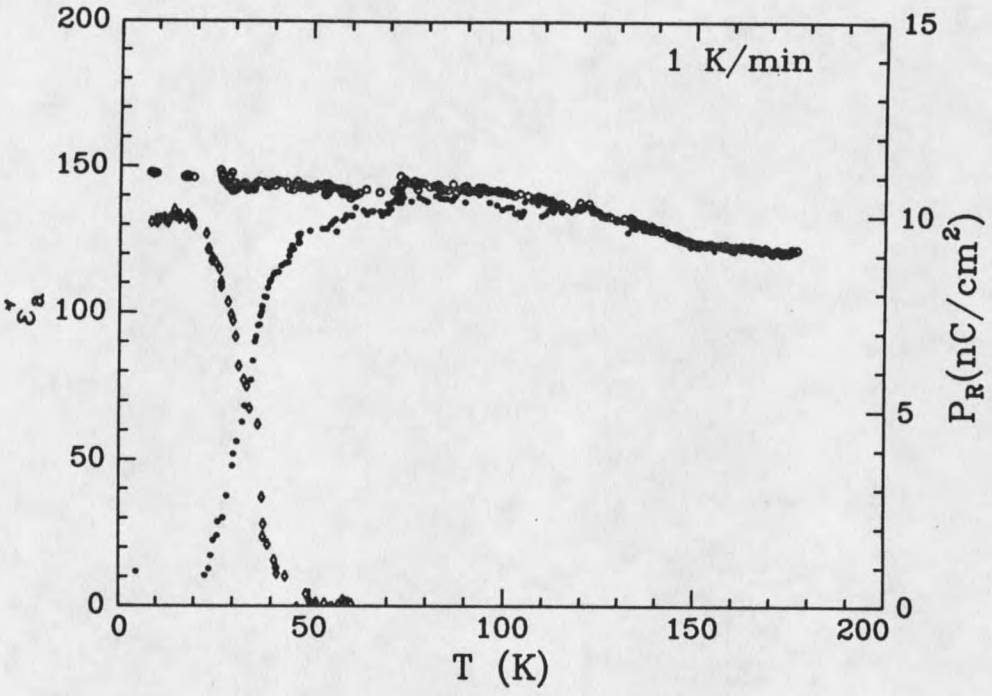

Figure 30. Temperature dependence of the field-cooled (o) and zero-field-cooled (•) static dielectric constant (left scale) of DRADA with x=0.28 measured along the a axis. The remanent polarization P_R (◊) is also shown (right scale). The electric field applied was 500 V/cm and the heating/cooling rate was 1 K/min.

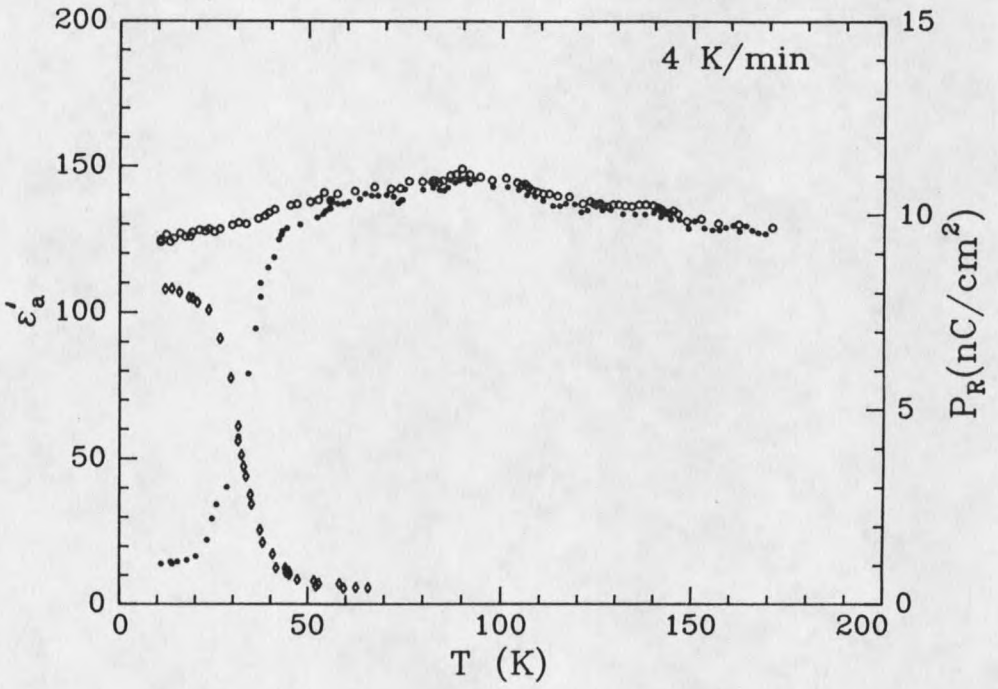

Figure 31. Temperature dependence of the field-cooled (o) and zero-field-cooled (•) static dielectric constant (left scale) of DRADA with x=0.28 measured along the a axis. The remanent polarization P_R (◊) is also shown (right scale). The electric field applied was 500 V/cm and the heating/cooling rate was 4 K/min.

The system is ergodic in this region and exhibits dielectric relaxation with frequency dispersion. Initially when the system is cooled without an external field the random freezing of the deuterons results in zero net polarization. In the presence of an external electric field the deuterons are biased to occupying one end of the bond as opposed to the other as temperature is raised and they gain additional energy. This results in the susceptibility building up until the paraelectric phase is reached above T_g. In this phase $\chi_{FC}=\chi_{ZFC}$. Below T_g the system does not obey the Curie-Weiss law and here $\chi_{FC}>\chi_{ZFC}$. Even above T_g there is some deviation below Curie-Weiss curve because of random bias tending to freeze out the response. This freezing causes χ_{FC} to tend to become horizontal as T->0, over and above the effects of nonergodicity. The zero-field-cooled susceptibility in this case is similar to the low frequency limit of the ac susceptibility which exhibits a rounded maximum as seen in Figure 23. The field-cooled susceptibility established by the external field retains the same value with a slight change of slope, as temperature is lowered below T_g and continues to remain constant as temperature is decreased due to the gradual freeze-out of the acid deuteron in the O-D...O bond. A remanent polarization is observed upon switching the field off. This polarization vanishes as temperature is raised

above T_g due to the thermal motion of the dipoles in their corresponding random local electric field environments. As seen in Figures 30 and 31, the remanent polarization at the slower heating and cooling rate (1 K/min) remains constant upon heating and drops above 20 K, while it begins to drop earlier for the faster heating and cooling rate (4 K/min). The maximum value of the remanent polarization is also seen to be higher for the slower heating and cooling rate (1 K/min) indicating greater order of the acid deuterons in polar Slater configurations. The remanent polarization obtained from field-cooling the sample is found to decrease faster when the heating rate is high. The maximum value of the remanent polarization is lower for faster heating and cooling rates. These results indicate a lesser order of the acid deuterons during the field-cooling process. Our values for ε_a' from both the dielectric and field-cooling experiments agree reasonably well, this by comparing Fig. 23 with Figs. 30 and 31.

Field-cooling experiments were conducted for deuterated and undeuterated crystals with smaller ammonium concentrations that show coexistence as seen in the previous two sections of this chapter. The static susceptibility and remanent polarization however were too small to measure without significant experimental errors like eliminating the voltage drift in the electrometer.

Based on the results obtained for the pure deuteron glass with x=0.28, it would be interesting to determine the variation of the susceptibility in the temperature region $T_g<T<T_c$. This would support our claim that below T_c we have intimate coexistence of ferroelectric domains with paraelectric clusters. Below T_g the behavior should be similar to the results obtained in this section.

Nuclear Magnetic Resonance

Nuclear magnetic resonance was performed on a single crystal of DRADA. Because nuclear magnetic resonance probes the local environment of the nuclei under study, we hoped to see a superposition of results in the deuteron spectra, from the paraelectric and ferroelectric portions of the crystal at temperatures below the ferroelectric phase transition temperature. The crystal has 10% ammonium concentration which puts it in the coexistence regime of the phase diagram as seen in Fig. 13.

The experiment was performed on a deuterated single crystal of DRADA, with x=0.10. The crystal was oriented with the dc magnetic field perpendicular to the ferroelectric c axis (z-direction) and along one of the other two crystallographic axis. ^2H spin lattice relaxation times and spectra were measured at 28 MHz. A Fourier

transform 90° saturation pulse sequence was used. The acid and ammonium deuterons were excited independently of each other by making use of the splitting in the acid deuteron line at Θ_z=0°. The splitting of the deuteron lines in pure KDP is shown in Fig. 9. The ammonium deuterons were excited by a 90° pulse (22 μs) with the center frequency set on resonance while the acid deuterons were also excited by a 90° pulse (16 μs) with the center frequency shifted 40 kHz below resonance. The activation energies were calculated from the spin lattice relaxation times for the ammonium and acid deuterons on the high temperature side of the BPP-like T_1 minimum.

In the paraelectric phase for pure $(ND_4)D_2AsO_4$ (DADA), all ND_4 groups are equivalent. The environment of each ND_4^+ ion is identical and axially symmetric along the crystal c axis on the time scale of the NMR experiment. This is so because of the fast intrabond motion of the acid deuterons between the two possible equilibrium sites in the O-D...O bond. The fast hindered rotation[37] of the ND_4^+ groups is slow however as compared to the intrabond motion of the O-D...O deuterons, hence each D site in a given ammonium ion experiences the same time-averaged electric field gradient (EFG) tensor which is axially symmetric. In the mixed crystal, the axial symmetry of the EFG is broken due to the random placements of Rb^+ and ND_4^+ ions. However at high

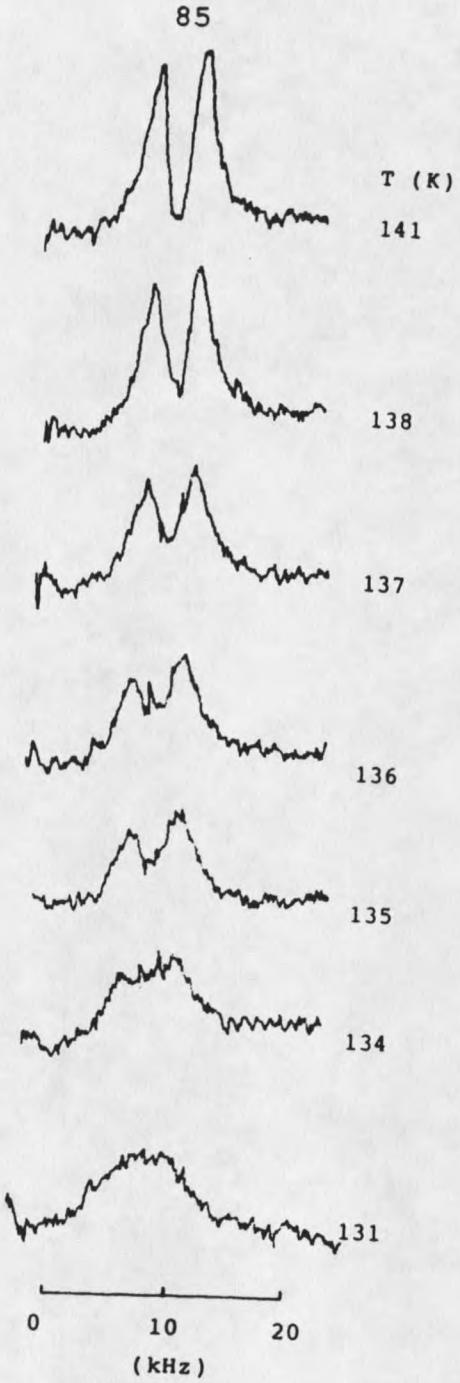

Figure 32. Temperature dependence of the ND_4^+ deuteron spectra. T_c for this sample is 146 K. Note the gradual build up of the broad component due to the ferroelectric phase.

temperatures, the ND_4 rotation about the c axis is fast enough that one of the principal axis of the EFG tensor is still along c.

The temperature dependence of the ND_4^+ deuteron Fourier transform NMR spectra are shown in Fig. 32. From 300 K down to 135 K the spectrum is a doublet which can be described as a superposition of two Gaussians displaced by 4 kHz. The doublet arises because ^2H is a spin 1 particle and so has three quantum energy levels and the splitting is present due to the interaction of the ^2H nucleus with the EFG. The width of the gaussians increases with decreasing temperature, however their separation and position are practically temperature independent. Below 135 K the doublet disappears due to the broadening of the individual gaussians. This broadening is a result of the random bias fields that get stronger as temperature is lowered. At still lower temperatures the ND_4 rotation slows down. The NMR signal at this piont was too small to analyze, however we should expect to see the rigid lattice spectra of the ND_4^+ deuterons because the specrum is no longer rotationally averaged. The ND_4^+ doublet splitting observed at room temperature in DRADA is analogous to the one found in pure deuterated ADP. It is compatible with the axially symmetric ND_4^+ EFG tensor expected to be found in the paraelectric phase at the ammonium site if all the acid deuterons move

fast between the two equilibrium sites in the O-D...O bonds. From spin lattice relaxation times for the ND_4 deuterons, the activation energy for the reorientation process of the ammonium deuterons is found to be 150 meV from Fig. 33 where we plot the spin lattice relaxation time T_1 for the ND_4^+ deuterons as a function of temperature. This activation energy is similar to that reported by Blinc et al.[38] for the ammonium deuterons in the deuterated phosphates (160 meV). The T_1 minimum for the ammonium deuterons is driven by ammonium reorientations. The activation energy can also be computed from the T_1 minimum where for $\Delta m=\pm 1$ and ± 2 transitions we have $\omega\tau=0.6$:[39] and

$$\tau=\tau_o \exp(-E_a/kT) \qquad (5.5)$$

where τ_o is the preexponential factor and we assume is approximately 5×10^{-14} s. Using Eq.(5.5) with T=160 K from Fig. 33, the activation energy is found to be 145 meV in good agreement with the previous result. The ferroelectric transition temperature is 146 K.

From the ND_4 spectra we see a superposition of lines from the ferroelectric and paraelectric portions of the sample. The gradual disappearance of the doublet to a single broad line at 131 K indicates that below this temperature most of the crystal is in the ferroelectric